Desorption of micropollutant from superfine and normal powdered activated carbon in submerged-membrane system due to influent concentration change in the presence of natural organic matter: experiments and two-component branched-pore kinetic model

Long Pan [a], Akiko Nakayama [b], Yoshihiko Matsui [a]*, Taku Matsushita [a], and Nobutaka Shirasaki [a]

[a] Faculty of Engineering, Hokkaido University, N13W8, Sapporo 060-8628, Japan

[b] Graduate School of Engineering, Hokkaido University, N13W8, Sapporo 060-8628, Japan

* Corresponding author. Tel/fax: +81-11-706-7280

E-mail address: matsui@eng.hokudai.ac.jp

Research highlights

- Desorption kept effluent MIB concentrations at measurable levels.
- AC with low adsorptive removal capacity showed high relative MIB desorption rate.
- Two-component reversible-adsorption model described desorption kinetics in NOM water.
- Half-dosed superfine PAC showed similar adsorption-desorption kinetics to normal PAC.
- A branched-pore kinetic model described the effect of AC particle size on kinetics.

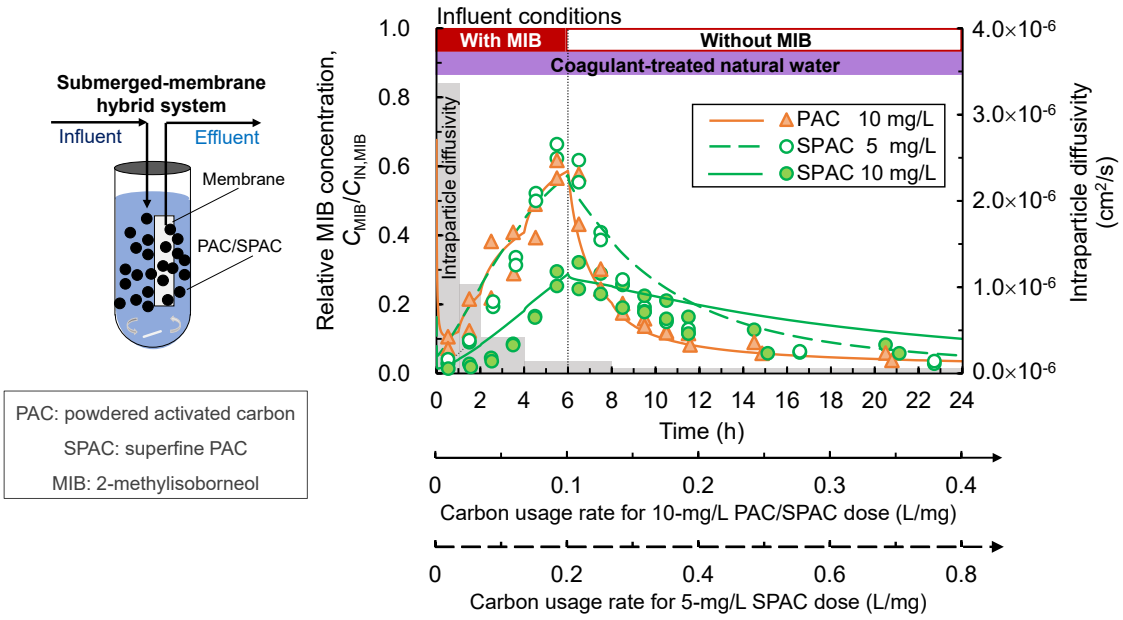

Abstract

Submerged-membrane hybrid systems (SMHSs) that combine membrane filtration with powdered activated carbon (PAC) take advantage of PAC's ability to adsorb and remove contaminants dissolved in water. However, the risk of contaminant desorption due to temporal changes in the influent concentration of the contaminant has not been thoroughly explored. In this study, we used a SMHS with conventionally-sized PAC or superfine PAC (SPAC) to remove 2-methylisoborneol (MIB), a representative micropollutant, from water containing natural organic matter (NOM), with the goal of elucidating adsorption–desorption phenomena in the SMHS. We found that 20–40% of the MIB that adsorbed on PAC and SPAC while the influent was contaminated with MIB (6 h, contamination period) desorbed to the liquid phase within 6 h from the time that the MIB-containing influent was replaced by MIB-free influent (no-contamination period). The percentage of desorption during the no-contamination period increased with increasing MIB breakthrough concentration during the contamination period. These findings indicate that the PAC/SPAC in the SMHS should be replaced while the breakthrough concentration is low, not only to keep a high removal rate but also to decrease the desorption risk. SPAC is fast in removal by adsorption, but it is also fast in release by desorption. SPAC (median diameter: 0.94 μm) showed almost the same adsorption-desorption kinetics as PAC (12.1 μm) of a double dose. A two-component branched-pore diffusion model combined with an IAST (ideal adsorbed solution theory)–Freundlich isotherm was used to describe and analyze the adsorption–desorption of MIB. The diffusivity of MIB molecules in the pores of the activated carbon particles decreased markedly in a short period of time. This decrease, which was attributed to fouling of the activated carbon in the SMHS by coagulant-treated water containing NOM, not only reduced the rate of MIB removal during the contamination period but also hindered the rate of MIB desorption during the no-contamination period and thus prevented the effluent MIB concentration from becoming high. On the other hand, coagulation did not change the concentration of NOM that competes with MIB for adsorption sites.

Keywords: 2-methylisoborneol, MIB, coagulation, microfiltration, MF, diffusion

Nomenclature

i, adsorbate *i* (MIB or EBC)

$C_i(t)$, concentration of adsorbate *i* in the effluent of the SMHS-PAC/SPAC (nmol/cm^3 = μmol/L) at time *t*

$C_{\mathrm{IN},i}$, concentration of adsorbate *i* in the influent of the SMHS-PAC/SPAC (nmol/cm^3 = μmol/L)

$c_{\mathrm{M},i}(t,r)$, liquid-phase concentration in the macropores of an AC particle at radial distance *r* and time *t* (nmol/cm^3 = μmol/L)

$D_{\mathrm{P},i}$, diffusion coefficient in macropores (cm^2/s)

$k_{\mathrm{f},i}$, external mass transfer coefficient (cm/s)

$k_{\mathrm{S},i}$, mass transfer rate coefficient in micropores (s^{-1})

$K_{\mathrm{LA},i}$, rate constant for loss due to volatilization (s^{-1})

$K_{\mathrm{F},i}$, Freundlich constant $\left[(\mathrm{nmol/mg})/(\mathrm{nmol/cm^3})^{1/n_{\mathrm{F},i}} = (\mathrm{\mu mol/g})/(\mathrm{\mu mol/L})^{1/n_{\mathrm{F},i}}\right]$

$n_{\mathrm{F},i}$, Freundlich exponent (dimensionless)

$q_i(t,r)$, solid-phase concentration (adsorbate loading per gram of AC) at radial distance *r* and time *t*, which is given by equation (1) (nmol/mg = μmol/g)

$q_{\mathrm{M},i}(t,r)$, adsorbate loading per gram of AC around macropore at radial distance *r* and time *t* (nmol/mg = μmol/g)

$q_{\mathrm{B},i}(t,r)$, adsorbate loading per gram of AC around micropore at radial distance *r* and time *t* (nmol/mg = μmol/g)

r, radial distance from the center of an AC particle (cm)

R, AC particle radius (cm)

t, time (s)

$C_{0,\mathrm{MIB}}$, initial concentration of MIB in a batch adsorption experiment (nmol/cm^3 = μmol/L)

$C_{0,\mathrm{EBC}}$, initial concentration of an EBC in a batch adsorption experiment (nmol/cm^3 = μmol/L)

$C_{\mathrm{E,MIB}}$, equilibrium liquid-phase concentration of MIB (nmol/cm^3 = μmol/L)

$C_{\mathrm{E,EBC}}$, equilibrium liquid-phase concentration of EBC (nmol/cm^3 = μmol/L)

C_{C}, AC dose (mg/cm^3 = g/L)

N, number of adsorbates (dimensionless)

Q, flow rate (cm^3/s)

$q_{E,MIB}$, equilibrium solid-phase concentration of MIB (nmol/mg = μmol/g)

$q_{E,EBC}$, equilibrium solid-phase concentration of EBC (nmol/mg = μmol/g)

V, volume of the submerged-membrane tank (cm^3)

ε, AC porosity (dimensionless)

ρ, AC particle density (mg/cm^3)

$\emptyset$, fraction of total adsorptive capacity available in macropores (dimensionless)

τ, tortuosity defined as the ratio of actual diffusion path length of a molecule to the shortest distance of its straight line (dimensionless)

AIC, Akaike information criterion

BIC, Bayesian information criterion

MSD, mean squared deviation

1. Introduction

Hybrid membrane systems for water treatment combine membrane filtration with another treatment process, such as photocatalysis, biodegradation, or adsorption, to remove dissolved micropollutants, including pesticides, pharmaceuticals and personal care products, taste-odor compounds, and natural organic matter (NOM). Systems that couple a low-pressure membrane with powdered activated carbon (PAC), thus combining the benefits of adsorptive removal by PAC and membrane separation of suspended particles (including the PAC), are used for water purification (Löwenberg et al., 2014; Shanmuganathan et al., 2017; Singh, 2005; Stoquart et al., 2012). In addition, the use of PAC prior to membrane filtration is also beneficial for urgent treatment of occasional pollution or treatment of emergency water supplies (Loo et al., 2012). PAC and superfine PAC (SPAC) not only adsorptively remove micropollutants but also reduce membrane fouling, thus enabling the attenuation of trans-membrane pressure rise and, consequently, reduction of the operational energy required for filtration (Amaral et al., 2016; Matsui et al., 2007; Matsui et al., 2009b; Tansakul et al., 2011; Xing et al., 2019).

In hybrid membrane systems, two methods for PAC application have been studied: continuous dose and pulse dose at the beginning of each filtration cycle (Campos et al., 2000a; Matsui et al., 2001; Schideman et al., 2002). Although the continuous-dose method is operationally simple, it is inefficient because the PAC added late in the filtration cycle has a short residence time in the reactor before being discarded, so it might not achieve as high an adsorption density as it would if it had been added earlier. Several researchers have compared the adsorption efficiencies of the pulse-dose and continuous-dose methods and reported the superiority of the pulse dose (Campos et al., 2000a, b; Matsui et al., 2001). In submerged-membrane filtration systems, a high-dose pulse of PAC is sometimes added to the membrane tank and retained there for at least several days to fully utilize the adsorption capacity of the PAC (Kim et al., 2007; Stoquart et al., 2012).

In most of previous studies of membrane hybrid systems, the influent concentrations of the compounds targeted for removal were constant ; that is, the studies did not account for temporal

changes in the influent concentration of the target compounds, which can occur with occasional pollutants. Meanwhile, the study of Löwenberg et al. (2014) should be noteworthy in that it is probably the only one observing the effect of influent concentration variation in hybrid membrane systems. They report that micropollutant removal rate was decreased after a peak load, attributing this decrease to desorption effect. In other words, as the influent concentration of a pollutant decreases, the pollutant adsorbed on the PAC held in the membrane tank can desorb, owing to the reversibility of adsorption. In addition, the presence of competitive adsorbates, such as NOM, may accelerate desorption of pollutants (Aschermann et al., 2018; To et al., 2008a, b).

The desorption of high-concentration adsorbates has been well studied (Banat et al., 2000; Chern and Wu, 2001; Martin et al., 2018). There have been several studies of micropollutant desorption from granular activated carbon (Corwin and Summers, 2011; Yuan et al., 2020), but the only study of desorption from PAC in hybrid membrane systems is that of Kim et al. (1996), who tested a single, high-concentration (higher than milligrams per liter) solution of dichlorobenzene in water. Very recent studies revealed that when the NOM concentration is low, when the activated carbon [AC] dosage is high, when AC is microporous with larger pore diameters, or when SPAC is used instead of PAC (all of which are conditions that minimize blockage of AC pores), the adsorption of micropollutants becomes more reversible (Aschermann et al., 2019a; Aschermann et al., 2019b; Aschermann et al., 2018; Nakayama et al., 2020): therefore, 100% desorption may occur at equilibrium when the liquid-phase concentration of the adsorbate is zero. However, studies of the kinetics of micropollutant desorption in the presence of NOM are rarely conducted because a complex analysis that goes beyond the application of the pore surface diffusion model for a single adsorbate is required (Newcombe et al., 2002; To et al., 2008a, b).

Compared with pressurized membrane filtration systems, submerged-membrane filtration systems retain PAC in the membrane tank at high concentrations for a relatively long time, the goal being to achieve sufficient utilization of PAC's adsorption capacity and/or to take advantage of PAC as a biological carrier (Stoquart et al., 2014; Stoquart et al., 2012); however, long retention of PAC entails the risk that even if the influent concentration sufficiently decrease, the effluent concentration

will remain high due to desorption as Löwenberg et al. (2014) report.

Given these considerations, our objectives in this study were to analyze the desorption of a micropollutant in a submerged-membrane hybrid system (SMHS) with a pulse AC dose not only experimentally but also theoretically by means of a two-component branched-pore kinetic model (BPKM), which enabled us to describe competitive adsorption of two compounds (the micropollutant and NOM) on ACs with different particle sizes. As adsorbents, we used SPAC with a median diameter of 0.94 μm and conventionally sized PAC with a median diameter of 12.1 μm; and we used 2-methylisoborneol (MIB), a representative micropollutant, as the target micropollutant.

2. Materials and methods

2.1. AC and coagulant

Commercially available wood-based PAC (median diameter, 12.1 μm; Taikou-W, Futamura Chemical Industries Co., Gifu, Japan) was slurried in ultrapure water (Milli-Q Advantage, Millipore Co.). Half of the slurry was milled with a wet bead mill (LMZ015, Ashizawa Finetech, Chiba, Japan) to generate superfine particles (median diameter, 0.94 μm; SPAC). Polyaluminum chloride (PACl) with basicity of 1.7 and a sulfate ion content of 2.8 wt % (250A, Taki Chemical Co., Hyogo, Japan) was diluted with ultrapure water to 23.7 mg-Al/L in the coagulant tank before use. The characteristics of the carbon are presented elsewhere (Matsui et al., 2015) and in Table 1S and Fig. 1S (Supplementary Information, SI).

2.2. Raw-water samples

Water collected from the Chibaberi River (Hokkaido, Japan) was filtered through a 0.2-μm PTFE membrane to remove any undissolved substances. Stock solutions of MIB were prepared by dissolving reagent-grade MIB (Wako Pure Chemical Industries, Osaka, Japan) in ultrapure water

193 and filtering the resulting solution through a 0.2-μm PTFE membrane filter.

194

195 We prepared the seven types of water samples for the experiments (Table 1 and Table 2S). NOM-
196 free water was prepared by adding inorganic salts to ultrapure water and adjusting the pH to ~7.0.
197 NOM-water was prepared by adjusting the pH of the filtered Chibaberi River water to pH 7.0. MIB-
198 spiked NOM-free water and MIB-spiked NOM-water were prepared by diluting the MIB stock
199 solution with NOM-free water and NOM-water, respectively, at around 1 or 0.1 μg/L. Coagulated
200 NOM-free water, Coagulated NOM-water, and Coagulated MIB-spiked NOM water were obtained
201 after NOM-free water, NOM-water, and MIB-spiked NOM-water, respectively, were subjected to
202 inline coagulation by means of a subsystem of the SMHS (as described in section 2.4). The MIB
203 concentrations 1 or 0.1 μg/L are higher than the concentrations commonly observed in water sources,
204 but such high concentrations of MIBs do occur in rare cases (Li et al., 2019; Liu et al., 2016;
205 Masakazu, 1988; Takahashi et al., 2016). In addition, the results of the evaluation in terms of relative
206 concentration can apply to normal low-concentration phenomena because the adsorption removal
207 percentages of trace contaminants such as MIB is independent from the influent concentration
208 (Gillogly et al., 1999; Graham et al., 2000; Knappe et al., 1998; Matsui et al., 2003). Furthermore,
209 the concentrations were set with the intention that low concentrations during desorption would be
210 measurable.

211

212 Table 1. List of waters used in experiments (details are presented Table 2S, SI)

	MIB (μg/L)	NOM (mg-C/L)	Coagulant (PACl) (mg-Al/L)
NOM-free water	0	0	0
MIB-spiked NOM-free water	1.18–1.37	0	0
Coagulated NOM-free water	0	0	2.0
NOM-water	0	4.85	0
MIB-spiked NOM-water	0.07–1.46	4.85	0
Coagulated NOM-water	0	3.21	2.0
Coagulated MIB-spiked NOM-water	0.08–1.17	3.21	2.0

213

214

215 **2.3. Determination of MIB concentrations**

216

217 MIB concentrations were determined by monitoring for MIB (*m/z* 95) with a headspace solid-phase
218 microextraction system (PAL RSI 85, Agilent Technologies Japan, Tokyo, Japan) coupled to a gas
219 chromatograph–mass spectrometer (7820A/5977 E MSD, Agilent); 2,4,6-trichloroanisole-d_3 (*m/z*
220 195, Wako Pure Chemical Industries, Osaka, Japan) was used as an internal standard. Details are
221 presented in the SI.

222

223 **2.4. SMHS with PAC/SPAC**

224

225 The small-scale SMHS shown in Fig. 1 was used for the experiments in this study. The system
226 consists of a raw-water tank, a coagulant tank, a submerged-membrane tank, a feed line consisting
227 of tubes and pumps, and an effluent collector. In addition, a subsystem without a submerged-
228 membrane tank was also set up in parallel to produce and collect blank water samples. The details
229 of the SMHS configuration are listed in Table 3S.

230

231 Raw water containing MIB was supplemented with PACl (2 mg-Al/L) and mixed in a static mixer,
232 and the resulting coagulated water was fed to the submerged-membrane tank. Immediately after the
233 tank was filled with the coagulated water, it was spiked with a pulse-dose of PAC or SPAC, and
234 membrane filtration was allowed to proceed for 6 h (referred to hereafter as the contamination
235 period). The filtration flux was 0.069 m/h, and the hydraulic retention time of the submerged-
236 membrane tank was 46 min. After 6 h of membrane filtration, the MIB-containing raw water was
237 replaced by MIB-free raw water, and membrane filtration was continued for another 18-19 h
238 (referred to hereafter as the no-contamination period); total filtration time, 24–25 h. For the first 3
239 min after the membrane filtration started, the effluent was discarded because of the effect of water
240 replacement in the tubing. The effluent fractions were collected consecutively: one 57-min fraction
241 (taken from 3 to 60 min), eleven 1-h fractions (taken from 1 to 2 h, 2 to 3h, etc.), one 5-h fraction,
242 and one 7-h fraction (in some runs, a 5-h fraction planned became a 10-h fraction, and then a 7-h

fraction became a 2-h fraction or a 3-h fraction, Fig. 2S). Concurrently, blank samples were collected every hour for the first 6 h. The collected samples were filtered through a 0.2-μm PTFE membrane (DISMIC-25HP; Toyo Roshi Kaisha, Tokyo, Japan) for MIB analysis. To compensate for the lack of multiple measurements for each sample due to the limited sample volumes, we collected many samples in succession and observed the time course of the MIB concentration to confirm that there were no outliers. In addition, SMHS experiments were conducted at two different dosages for each AC. The two dosages were 10 and 20 mg/L for PAC and 5 and 10 mg/L for SPAC. For each condition except 20-mg/L dosage, two experiments were performed to confirm the reproducibility of the results. The AC dosage was defined as the mass of AC divided by the volume of the water treated during the contamination period. All experiments, including analyses of water quality, were conducted in a room with a constant temperature of ~20 °C.

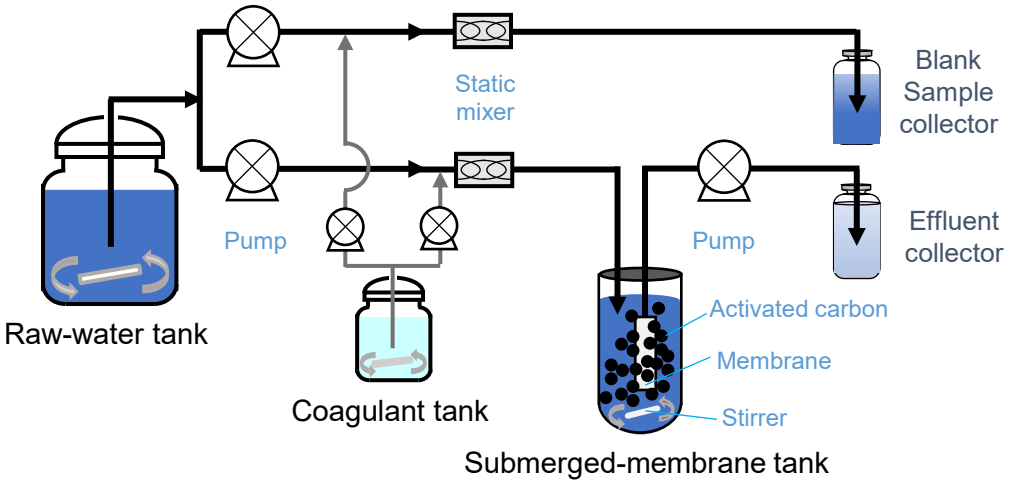

Fig. 1. Schematic diagram of the SMHS(submerged-membrane hybrid system)-PAC(powdered activated carbon)/SPAC(superfine powdered activated carbon) used in this study.

2.5. Batch adsorption equilibrium tests

For batch adsorption equilibrium tests, vials containing raw water (Table 2S) were spiked with specified amounts of AC (0.5–16 mg/L), sealed, manually shaken, and then agitated on a mechanical

shaker at a constant temperature of 20 °C in the dark for 2 weeks, which was sufficient for achieving adsorption equilibrium (Nakayama et al., 2020). In single-solute MIB adsorption equilibrium tests, 110-mL aliquots of MIB-spiked NOM-free water in 115-mL vials were used. In the MIB adsorption equilibrium tests in the presence of NOM, 65-mL aliquots of MIB-spiked NOM-water and Coagulated MIB-spiked NOM-water in 68-mL vials were used. All the vials were cleaned and dried at 550 °C before use. After 2 weeks, the contents of the vials were filtered through 0.2-μm membrane filters, and MIB concentrations in the aqueous phase were measured. Solid-phase MIB concentrations were calculated based on mass balance.

2.6. Adsorption-desorption model for the SMHS-PAC/SPAC

2.6.1. Development of a model for multicomponent adsorption-desorption kinetics in the submerged-membrane tank

We constructed a multicomponent model for the kinetics of adsorption-desorption of MIB molecules on the PAC/SPAC in the SMHS by using the BPKM of Peel et al. (1981). The BPKM divides carbon particle into two regions of different diffusion rates, which are loosely termed macropores and micropores (note: these terms should not be confused with their conventional uses to define certain pore size ranges). The BPKM consisted of three mass transfer resistances in series (Fig. 3S): passage of adsorbates across the external surface of an AC particle, intraparticle diffusion of the adsorbates in the macropores, and mass transfer from the macropore to the micropores. The model equations are briefly described as follows (details are in SI).

Since the parts of the total adsorptive capacity which are utilized in macropores and micropores are $\emptyset$ and $(1-\emptyset)$, respectively, the adsorbate loading per gram of AC (solid phase concentration) is given by:

$$q_i(t,r) = \emptyset q_{\mathrm{M},i}(t,r) + (1-\emptyset) \times q_{\mathrm{B}.i}(t,r) \quad (1)$$

Here, it was assumed that the macropores and micropores are uniformly distributed throughout the particles (Peel et al., 1981). Therefore, $\emptyset$ is not a function of the radial direction, but is treated as a constant value.

The mass balance in micropore is as follows:

$$\frac{\partial q_{\mathrm{B},i}(t,r)}{\partial t} = \frac{k_{\mathrm{S},i}}{1-\emptyset}\left[q_{\mathrm{M},i}(t,r) - q_{\mathrm{B},i}(t,r)\right] \quad (2)$$

The mass balance in macropores is as follows:

$$\frac{\partial q_{\mathrm{M},i}(t,r)}{\partial t} = \frac{\varepsilon D_{\mathrm{P,i}}}{\rho r^2}\frac{\partial}{\partial r}\left[r^2\frac{\partial c_{\mathrm{M,i}}(t,r)}{\partial r}\right] - \frac{k_{\mathrm{S},i}}{\emptyset}\left[q_{\mathrm{M},i}(t,r) - q_{\mathrm{B},i}(t,r)\right] \quad (3)$$

A CSTR (continuous stirred tank reactor) model is applied to describe the mass balance equation for an adsorbate in a membrane tank.

$$\frac{\mathrm{d}C_i(t)}{\mathrm{d}t} = -\frac{3C_{\mathrm{C}}k_{\mathrm{f},i}}{\rho R}\left[C_i(t) - c_{\mathrm{M},i}(t,R)\right] + C_{\mathrm{IN},i}\frac{Q}{V} - C_i(t)\frac{Q}{V} - K_{\mathrm{LA},i}C_i(t) \quad (5)$$

Local adsorption equilibrium in the macropores of an AC particle is expressed by the IAST (ideal adsorption solution theory)–Freundlich isotherm equation (Crittenden et al., 1985; Hand et al., 1985). It should be noted that the use of the adsorption equilibrium equation implicitly assumes that adsorption is reversible, that is, that 100% desorption occurs when the liquid-phase concentration goes to zero.

2.6.2. Isotherm parameter estimation method

To describe competitive adsorption of background NOM and MIB, we used an equivalent

background compound (EBC) method (Graham et al., 2000; Najm et al., 1991; Newcombe et al., 2002), where the EBC is a hypothetical compound that represents the NOM that competes with the target compound (MIB in this research) for adsorption sites. The mass balance in a vial used for batch adsorption experiments was as follows:

$$C_{0,\mathrm{MIB}} - q_{\mathrm{E,MIB}}\, C_{\mathrm{C}} = \frac{q_{\mathrm{E,MIB}}}{q_{\mathrm{E,MIB}} + q_{\mathrm{E,EBC}}} \left(\frac{q_{\mathrm{E,MIB}}\, n_{\mathrm{F,MIB}} + q_{\mathrm{E,EBC}}\, n_{\mathrm{F,EBC}}}{K_{\mathrm{F,MIB}}\, n_{\mathrm{F,MIB}}} \right)^{n_{\mathrm{F,MIB}}} \quad (7)$$

$$C_{0,\mathrm{EBC}} - q_{\mathrm{E,EBC}}\, C_{\mathrm{C}} = \frac{q_{\mathrm{E,EBC}}}{q_{\mathrm{E,MIB}} + q_{\mathrm{E,EBC}}} \left(\frac{q_{E,\mathrm{MIB}}\, n_{\mathrm{F,MIB}} + q_{E,\mathrm{EBC}}\, n_{\mathrm{F,EBC}}}{K_{\mathrm{F,EBC}}\, n_{\mathrm{F,EBC}}} \right)^{n_{\mathrm{F,EBC}}} \quad (8)$$

In the EBC method, the equations are repeatedly solved by assuming those for EBC ($C_{0,\mathrm{EBC}}$, $K_{\mathrm{F,EBC}}$, and $n_{\mathrm{F,EBC}}$) to search for the best fit of the calculated MIB concentrations to the experimentally observed concentrations. We conducted searches to minimize the *MSD*, which corresponds to the average of relative squared errors between the observed and calculated concentrations.

3. Results and discussion

3.1. Adsorption-desorption kinetics in the SMHS-PAC/SPAC

When the SMHS-PAC/SPAC was operated for 24 h with a pulse AC dose, the MIB concentration in the effluent increased with time for the first 6 h (the contamination period), during which the influent water contained MIB (Coagulated MIB-spiked NOM-water). Even after the influent MIB concentration dropped to zero (that is, during the no-contamination period after the Coagulated MIB-spiked NOM-water was replaced by Coagulated NOM-water or Coagulated NOM-free water), the MIB concentration in the effluent remained high for a time and continued to be detectable throughout all the runs (Figs. 2 and 3). The effluent concentration dropped faster in the SMHS without AC (Fig. 5S). This difference indicates that the high MIB concentrations observed in the

effluents during the no-contamination period in the presence of AC were due to desorption of MIB that had been adsorbed on the AC during the contamination period; that is, the MIB was supplied to the liquid phase from the solid phase.

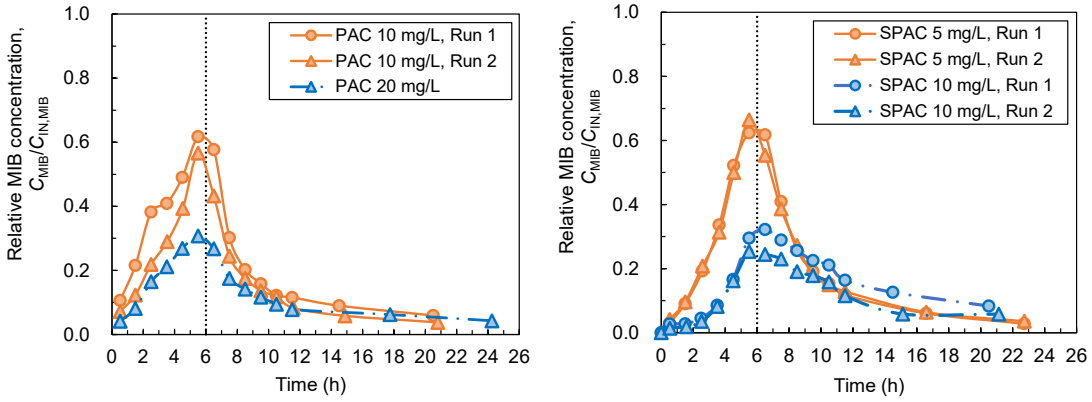

Fig. 2. Time course of effluent/influent MIB concentration ratios ($C_{MIB}/C_{IN,MIB}$) in the SMHS with two different dosages of PAC (left) and SPAC (right). The MIB-containing influent (Coagulated MIB-spiked NOM-water, $C_{IN,MIB} \approx 1$ μg/L) was replaced by MIB-free influent (Coagulated NOM-water) at 6 h (vertical dotted lines). The x-axis values of the plots are times in the middle of each sampling period.

Two different dosages were tested for each AC (10 and 20 mg/L for PAC; 5 and 10 mg/L for SPAC). The effluent MIB concentration during the contamination period was lower at the higher AC dosages than at the lower AC dosages, and the concentration continued to be lower for some time after the influent MIB concentration dropped to zero (compare the orange and blue curves in Fig. 2). For SPAC, the effluent MIB concentrations late in the no-contamination period became higher at the high AC dosage than that at the low AC dosage. The reason for this is that at the higher AC dosages, more MIB was removed from the water during the contamination period, and therefore more was desorbed during the no-contamination period, in particular for SPAC which adsorbs and desorbs MIB at a faster rate than PAC. Desorption, including observed desorption percentage (around 50% or less) and ultimate desorption percentage, is more discussed in sections 3.2.3 and 3.2.4, which deal with the model fitting and simulation.

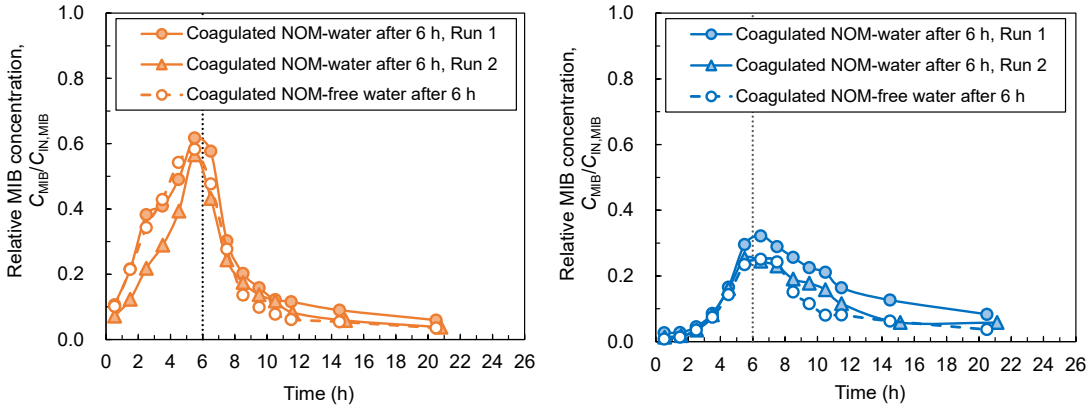

Fig. 3. Time course of effluent/influent MIB concentration ratios ($C_{MIB}/C_{IN,MIB}$) in the SMHS with 10 mg/L PAC (left panel) and 10 mg/L SPAC (right panel). The solid and dashed lines indicate data for tests in which MIB-containing influent (Coagulated MIB-spiked NOM-water, $C_{IN,MIB} \approx 1$ μg/L) was replaced by MIB-free water, either Coagulated NOM-water or Coagulated NOM-free water, respectively, at 6 h (vertical dotted lines). The x-axis values of the plots are times in the middle of each sampling period.

When Coagulated NOM-free water, which contained neither MIB nor NOM, was used to replace Coagulated MIB-spiked NOM-water as the influent after the initial 6 h of the test, the MIB concentrations in the effluents decreased (Fig. 6S c and f). However, the concentrations were lower than the concentrations when Coagulated NOM-water was used (Fig. 3). These results indicate that not only the decrease of the MIB influent concentration but also the presence of NOM caused desorption of MIB previously adsorbed on the AC. Notably, in the blank tests of the SMHS without AC, the MIB concentration in the effluent was 15.6% lower than in the influent (Fig. 5S), a result that we attributed to loss due to volatilization of MIB from the submerged-membrane tank of the SMHS.

During the contamination period, a given dose of SPAC removed a similar amount of MIB as a PAC dose that was twice as high (Figs. 2 and 7S); compare PAC at 10 mg/L to SPAC at 5 mg/L and

compare PAC at 20 mg/L to SPAC at 10 mg/L. In a previous study of a pressurized membrane filtration-adsorption system (Matsui et al., 2007), we found that 4 times as much PAC as SPAC was necessary to remove the same amount of geosmin, a typical micropollutant with a molecular weight and hydrophobicity similar to those of MIB. The smaller difference between the required PAC and SPAC dosages in the current study can be attributed not only to the faster intraparticle diffusivity of MIB compared with that of geosmin but also to the relatively longer AC–water contact time (46 min, Table 3S) in the SMHS, which attenuated the effect of the faster adsorption kinetics of SPAC, than that in a pressurized membrane filtration-adsorption system (4–9 min), as the effect of contact time on PAC/SPAC is discussed by Matsui et al. (2013).

From the mass balance of MIB in the SMHS-PAC/SPAC (Table 4S), we calculated the concentration of MIB adsorbed on AC (solid-phase MIB concentration) and plotted it as a function of time (Fig. 4). The solid-phase concentration increased during the contamination period (6 h) and then decreased after the MIB-containing influent water was replaced with MIB-free NOM water (no-contamination period). Approximately 20–40% of the MIB adsorbed during the contamination period desorbed during the first 6 h of the no-contamination period (Figs. 4 and 8S). The percentage of desorbed MIB increased with time, reaching 40–55% after 24 h (18 h after the influent switch). However, MIB desorption had slowed with time, and it seemed that it might take many days before all the MIB released, or a substantial fraction of the MIB might adsorb irreversibly. Notably, Aschermann et al. (2018), Aschermann et al. (2019b) and Nakayama et al. (2020) reported nearly 100% reversibility of micropollutant adsorption: specifically, they found that adsorption of micropollutants is almost completely reversible under equilibrium conditions with a low background NOM concentration, a high AC dosage, or AC with large pores. Considering the low NOM concentration and high AC dosage in our experiments, it is possible that, all of the MIB preadsorbed on the AC might be desorbed after MIB-free water had been fed to the SMHS-PAC/SPAC for >>24 h.

The MIB desorption percentages were higher with NOM water than with NOM-free water (Fig. 8S) because of competitive adsorption of the NOM (that is, displacement of MIB molecules by NOM

molecules) (Aschermann et al., 2018; Nakayama et al., 2020). The desorption percentages were higher at the lower AC dosages (Figs. 4 and 8S). Low AC dosages resulted in high solid-phase MIB concentrations (high MIB loading on AC), which could have accelerated desorption.

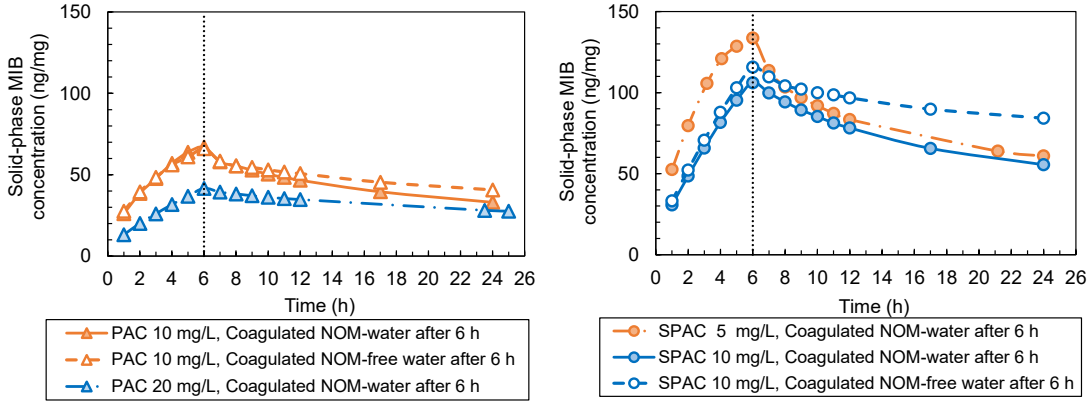

Fig. 4. Time course of solid-phase MIB concentrations (i.e., MIB adsorbed on AC) in the SMHS with PAC (left) and SPAC (right). The MIB-containing influent (Coagulated MIB-spiked NOM-water, $C_{IN,MIB} \approx 1$ μg/L) was replaced by MIB-free influent (either Coagulated NOM-water or Coagulated NOM-free water) at 6 h (vertical dotted lines).

3.2. Model simulation of adsorption-desorption of MIB on PAC/SPAC in the SMHS.

3.2.1. Adsorption equilibrium of MIB in the presence of NOM

The single-solute isotherms for MIB adsorption on PAC and SPAC were nearly identical (Fig. 5). Because the isotherms were similar, we applied the same MIB adsorption isotherm parameter values for PAC and SPAC, which resulted in a Freundlich constant ($K_{F,MIB}$) of 0.114 $(\mu mol/mg)/(\mu mol/L)^{1/n_{F,EBC}}$ and a Freundlich exponent ($1/n_{F,MIB}$) of 0.472.

The isotherms for the MIB-spiked NOM-water and the Coagulated MIB-spiked NOM-water were nearly identical (Fig. 5), indicating that addition of the coagulant (PACl) did not affect the MIB adsorption capacity of either PAC or SPAC and did not change the concentration of NOM that competes with MIB for adsorption sites. This finding is in agreement with that reported by Altmann

et al. (2015) for PAC and is reasonable in light of previous reports that (1) treatment with aluminum coagulants including PACl does not work with low-molecular-weight NOM (Fig. 4S) (Sillanpää, 2014; Yan et al., 2008) and (2) low-molecular-weight NOM has the strong inhibitory effect among other NOMs on MIB adsorption, and natural organic matter that competes with MIB for adsorption sites is such NOM (Ho and Newcombe, 2005; Matsui et al., 2003; Newcombe et al., 2002). Moreover, the influences of NOM on MIB adsorption by PAC and SPAC were similar, and therefore the MIB isotherms for the two NOM waters were almost the same for PAC and SPAC, as was the case for the single-solute isotherms.

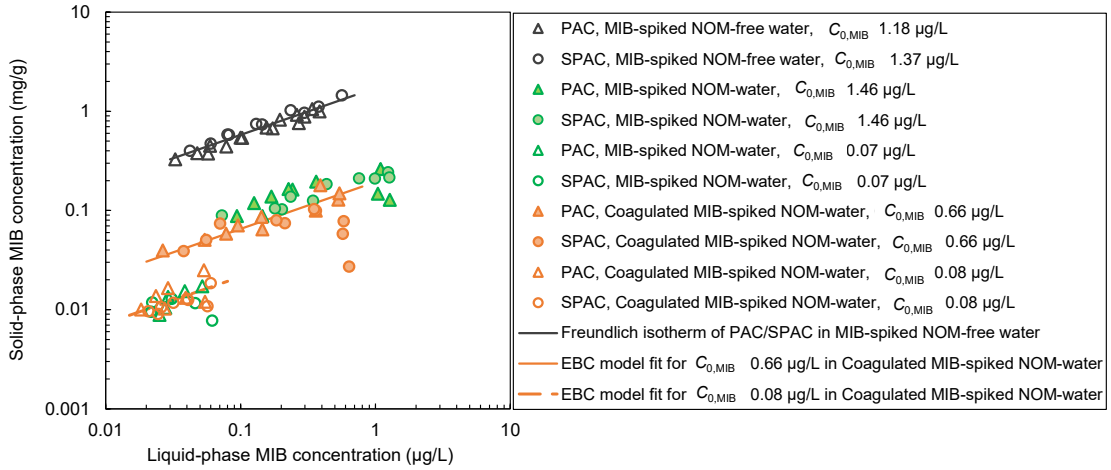

Fig. 5. Isotherms for adsorption of MIB on PAC and SPAC from MIB-spiked NOM-free water, MIB-spiked NOM-water, and Coagulated MIB-spiked NOM-water.

3.2.2. Parameter value evaluation for adsorption isotherm

The EBC method for fitting the isotherm of a micropollutant in the presence of NOM typically involves a search for three parameter values: the initial liquid-phase concentration ($C_{0,EBC}$), the Freundlich constant ($K_{F,EBC}$), and the Freundlich exponent ($n_{F,EBC}$) of the EBC (NOM) (Najm et al., 1991). Since determining unique values for $K_{F,EBC}$ and $n_{F,EBC}$ is often difficult (Graham et al., 2000; Knappe et al., 1998; Qi et al., 2007), we used the EBC method under three conditions (A–C, Table

2). The *AIC* (Akaikes information criterion) and *BIC* (Bayesian information criterion) (Akaike, 1974; Burnham and Anderson, 2002; Schwarz, 1978) values indicated that the most reasonable isotherm fitting was achieved under condition C (details are in SI). The isotherm fits were also visually confirmed (Fig. 9S). The assumption of condition C that $K_{F,EBC}$ and $n_{F,EBC}$ were the same as $K_{F,MIB}$ and $n_{F,MIB}$, respectively, was appropriate because the values obtained for EBC under conditions A and B were similar to the MIB values.

The estimated EBC concentration (0.223 μmol/L) was much higher than the MIB concentration (0.006 μmol/L) and was lower than the total NOM concentration (~ 3.2 mg/L, Table 2S); these results are consistent with the fact that the EBC concentration is generally much higher than the target micropollutant (MIB) concentration and that the EBC constitutes only a portion of NOM (Edzwald, 2010; Knappe et al., 1998; Matsui et al., 2003). EBC concentration was almost the same between MIB-spiked NOM-water and Coagulated MIB-spiked NOM-water, which clearly indicates that little EBC was removed by coagulation, as inferred from section 3.2.1.

Table 2. EBC parameters and *MSD*, *AIC*, and *BIC* values for the three search conditions.

	Coagulated MIB-spiked NOM-water			MIB-spiked NOM-water
Parameter/value (unit)	Condition A	Condition B	Condition C	Condition C
EBC parameters				
$C_{0,EBC}$ (μmol/L)	0.224	0.210	0.223	0.247
$K_{F,EBC}$ (μmol/mg)/(μmol/L)$^{1/n_{F,EBC}}$	0.141	0.133	0.114 (fixed)	0.114 (fixed)
$1/n_{F,EBC}$ (dimensionless)	0.486	0.472 (fixed)	0.472 (fixed)	0.472 (fixed)
MSD (dimensionless)	0.0273	0.0273	0.0280	0.0332
AIC (dimensionless)	−120	−122	−123	−100
BIC (dimensionless)	−115	−119	−122	−98.8

EBC refers to the equivalent background compound. *MSD* refers to the mean squared deviation. *AIC* refers to the Akaikes information criterion. *BIC* refers to the Bayesian information criterion.

3.2.3. Model simulation of the kinetics of adsorption-desorption in the SMHS-PAC/SPAC

Some of the parameters required for the BPKM simulation were predetermined from experiments independent of the SMHS experiments or from literatures. These parameters and the methods by which they were determined are presented in Table 5S. As mentioned in section 3.2.2, we assumed that the EBC molecule was similar in size to MIB and thus that the external mass transfer coefficients, pore diffusion coefficients, and micropore mass transfer coefficients were the same for MIB and EBC. Finally, five unknown parameters remained. For these five parameters, we evaluated seven different search settings, and the parameter values were optimized for each setting. The simulation results of the parameter search settings are summarized in Table 3.

The details of the simulation results are described in SI, but the main points are as follows. The simulation results obtained with settings A to E and G did not fit the experimental data (Fig. 10S-15S). The discrepancies suggested the change in intraparticle diffusivity due to the adsorption of NOM by the AC or to the effects of coagulant, such as AC flocculation and hindrance of mass transfer/diffusivity by the aluminum precipitate (Ho and Newcombe, 2005; Sidney Seckler et al., 2013; To et al., 2008a, b). After all, setting F, which takes into account the effects of NOM loading and/or coagulation in such a way that the pore diffusion coefficient in an AC particle is assumed to decrease with the residence time of the AC in the SMHS, gave the best fit to the experimental data with the smallest *MSD* value. Compared with the other settings, setting F has more parameters, so the better fit may not be particularly surprising. However, despite the larger number of parameters, preference should be given to setting F because it yielded the minimum values of both *AIC* and *BIC* values. These results suggest that the decrease in uptake rate of MIB is related to the change in internal diffusion (D_P), not to the external mass transfer (k_f), and that the decrease in internal diffusion is not related to the amount of EBC adsorbed. The latter is consistent with previous findings that pore blockage is caused by large NOM molecules rather than small NOM molecules (To et al., 2008a, b).

Table 3. Optimized model parameters and *MSD*, *AIC*, and *BIC* values for various search settings.

	Setting A	Setting B	Setting C	Setting D	Setting E	Setting F	Setting G
	Pore diffusion model		Branched pore kinetic model				
$k_{f,\,PAC}$ (cm/s)	1.50	0.98	0.81	2.81	1.0 (fixed)	1.0 (fixed)	Changes with time (h) 0.927 (0–1) 0.075 (1–2) 0.003 (2–6) 0.027 (6–24)
$k_{f,SPAC}$ (cm/s)		1.11		1.94			
D_P (cm^2/s)	1.71×10^{-7}	1.72×10^{-7}	5.00×10^{-7}	5.03×10^{-7}	Changes with EBC loading (µmol/g-AC) 1.57×10^{-6} (0–4) 1.49×10^{-6} (4–8) 2.09×10^{-7} (8–12) 2.06×10^{-7} (12–15) 2.04×10^{-7} (>15)	Changes with time (h) 3.32×10^{-6} (0–1) 1.03×10^{-6} (1–2) 4.22×10^{-7} (2–4) 1.25×10^{-7} (4–8) 6.67×10^{-8} (8–24)	6.68×10^{-7}
ϕ (dimensionless)	Not applicable	Not applicable	0.586	0.587	0.599	0.580	0.597
k_S (s^{-1})			9.72×10^{-6}	9.62×10^{-6}	8.36×10^{-6}	1.20×10^{-5}	9.71×10^{-6}
MSD	0.0033	0.0033	0.0019	0.0019	0.0017	0.0010	0.0019
AIC	-303	-301	-348	-346	-354	−402	-344
BIC	-298	-294	-338	-333	-337	−385	-326
Figure	Fig. 10S	Fig. 11S	Fig. 12S	Fig. 13S	Fig. 14S	Fig. 6	Fig. 15S

MSD refers to the mean squared deviation. *AIC* refers to the Akaikes information criterion . *BIC* refers to the Bayesian information criterion.

526

527

528

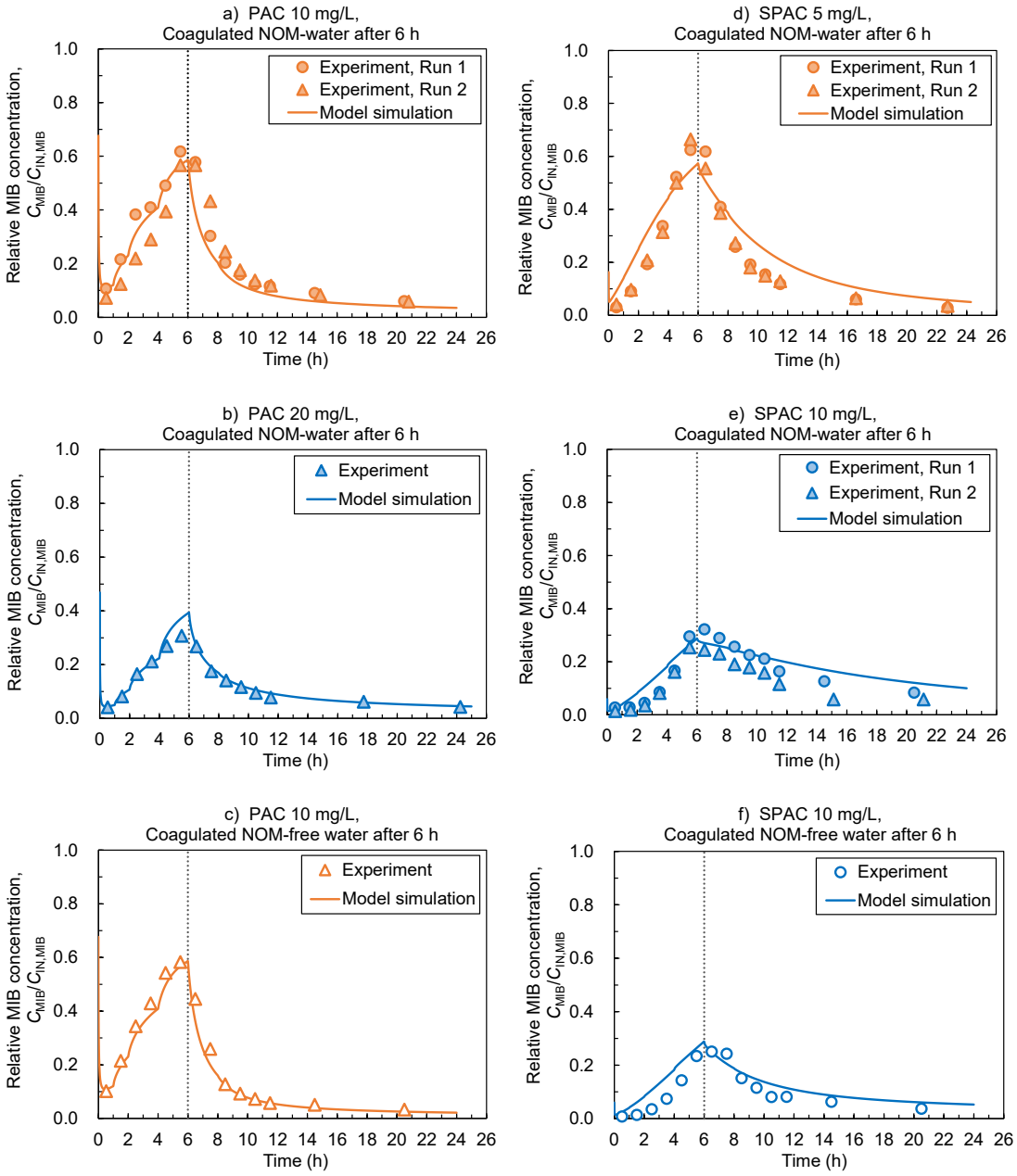

Fig. 6. Comparison of experimental and simulated time courses of effluent/influent MIB concentration ratios ($C_{MIB}/C_{IN,MIB}$) in the SMHS with PAC (left panels) and SPAC (right panels). Simulations were conducted using setting F. The MIB-containing influent (Coagulated MIB-spiked NOM-water, $C_{IN,MIB} \approx 1$ μg/L) was replaced by MIB-free influent (either Coagulated NOM-water or Coagulated NOM-free water) at 6 h (vertical dotted lines).

543 The D_P values estimated using setting F are shown in Fig. 7. The initial D_P value was 3.5×10^{-6}
544 cm^2/s, and the tortuosity (τ) estimated from this value was 1.9 (Table 6S). This tortuosity is
545 essentially consistent with previously reported values for virgin AC [2–4 (Ocampo-Pérez et al.,
546 2012), 3 (Corwin and Summers, 2011), 3.5 (Pan et al., 2016), 2-6 (Suzuki, 1990) and other values
547 (Sontheimer et al., 1988)]. The D_P value decreased markedly with time for the first 2 h, after which
548 the decrease continued but at a slower rate. The decrease in D_P indicates that AC fouling, which led
549 to constriction and blocking of the pores, occurred mostly in the first few hours. The total NOM
550 loadings on the ACs at the first 2 h ranged between 20 and 90 mg-C/g (Fig. 16S). According to
551 previous research, pore constriction and blocking occur at NOM loadings > ~50 mg-C/g, which
552 reduces the internal diffusivity by a factor of 10 or less (Li et al., 2003; To et al., 2008a). Therefore,
553 the AC fouling observed in our study could be related to the NOM loading. In addition, considering
554 the results of previous studies that reported that coagulation treatment (Ho and Newcombe, 2005)
555 and coating the outer surface of PAC with coagulant (Sidney Seckler et al., 2013) slowed the rate of
556 external mass transfer of trace contaminants to the PAC surface, and that incorporation of PAC into
557 floc particles did not inhibit external mass transfer (Altmann et al., 2015), this may also be related
558 to the addition of coagulant (PACl), which was used to remove NOM and attenuate membrane
559 fouling (Chen et al., 2020; Matsui et al., 2009b). Furthermore, the better model fit obtained with
560 setting F (changing D_P) over setting G (changing k_F) in our study suggests that the intraparticle pore
561 diffusion has been retarded more severely than external mass transfer. In this way, the AC fouling
562 led to a decrease in the rate of MIB removal in the SMHS-PAC/SPAC, although the fouling
563 prevented and delayed desorption of previously adsorbed MIB when the influent MIB concentration
564 decreased.
565
566

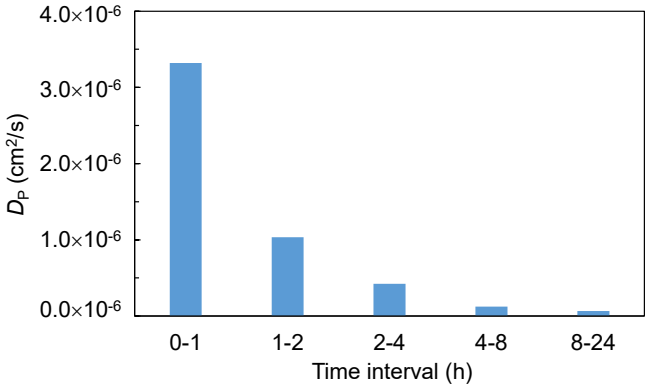

Fig. 7. Estimation of intraparticle diffusivity (D_P) in AC pores by means of best-fitting model simulation for setting F.

3.2.4. Analysis by the model simulation

The removal rate depends on the AC dosage, but in order to investigate how the desorption rate changes with the AC dosage, the experimental and simulation results are summarized in Fig. 8. Both the MIB desorption ratio and the MIB remaining proportion (effluent/influent concentration) decreased as the AC dosage was increased. These results can be interpreted as indicating that the lower the MIB removal rate was during the contamination period, and the more breakthrough that was detected in the effluent during that period, the higher the MIB desorption ratio was during the no-contamination period. Because desorption is caused by an inverse concentration gradient, it seems reasonable to expect that the absolute amount of desorption became high when the effluent concentration was high. However, the important point is that the ratio of the amounts of desorbed and adsorbed MIB becomes higher with higher effluent concentration. Therefore, when the influent concentration dropped and remained at low levels, the SMHS-AC with a low MIB removal rate had the disadvantages of having not only a high effluent concentration but also a high desorption ratio. In such a case, the AC in the SMHS should be drained, in particular when the remaining adsorption capacity of the AC is low, which leads to low adsorptive removal of micropollutants. This operational strategy is also important when AC is used for sporadic contaminant episodes, such as algae blooms and industrial spills.

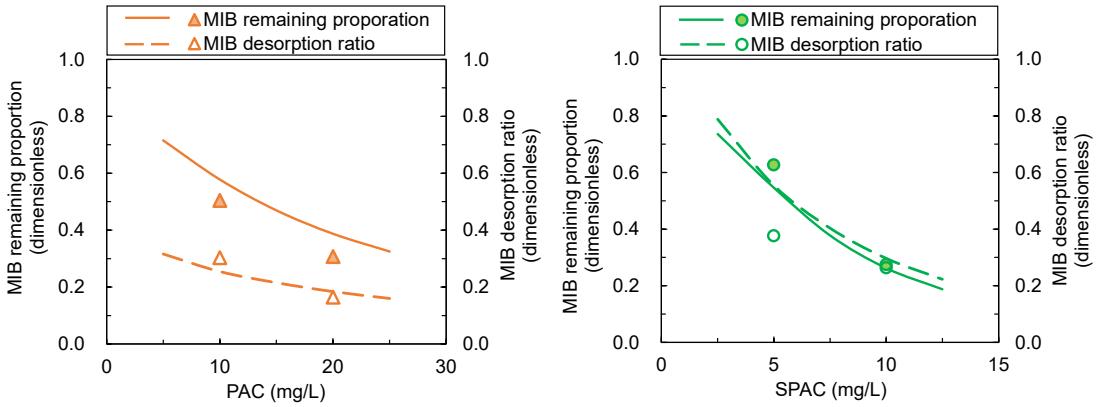

Fig. 8. Effects of PAC (left) and SPAC (right) dosage on MIB remaining proportion and MIB desorption ratio. The symbols indicate experimental data; the lines represent the data of model simulation by using optimized parameters of setting F. The MIB remaining proportions were determined at 6 h, just before the MIB-containing influent ($C_{IN,MIB}$ = 1 μg/L) was replaced by the MIB-free influent. The MIB desorption ratio is the ratio of the amount of MIB desorbed during the first 6 h of the no-contamination period divided by the amount of MIB adsorbed during the 6 h of the contamination period.

4. Conclusions

In a hybrid system that combines AC adsorption with a submerged-membrane filtration, we found that the micropollutant MIB desorbed from the AC when the influent MIB concentration decreased, and desorption was accelerated by the presence of NOM in the influent. Approximately 20–40% of the MIB that adsorbed on the AC during the first 6 h of the test was released over the course of the first 6 h after the MIB-containing water was replaced with natural water. When the effluent MIB concentration was high and the MIB removal rate just prior to the no-contamination period was low, the desorbed/adsorbed MIB ratio and the absolute amount of MIB desorption were high. These results indicate that the AC in the submerged-membrane tank should be replaced while the breakthrough concentration is low.

The MIB adsorption-desorption performances of PAC and SPAC in the SMHS were well described by a two-component (MIB and EBC) BPKM with the implicit assumption of 100% adsorption/desorption reversibility. The model fitting indicated that intraparticle diffusivity decreased largely over the course of a few hours of SMHS operation. This decrease in intraparticle diffusivity was expected to lead to earlier MIB breakthrough by decreasing the adsorption rate, and it also reduced the desorption rate of preadsorbed MIB and suppressed the effluent concentration when the influent MIB concentration decreased.

A given dose of SPAC showed almost the same adsorption-desorption kinetics as a PAC dose that was twice as high. Reduction in the AC particle size contributed to faster MIB adsorption and desorption, even though the adsorption capacities of the two different ACs were the same. The 2-fold difference between SPAC and PAC was smaller than the previously reported 4-fold difference observed for a pressurized membrane filtration system, a result that we attributed to the relatively longer AC detention time in the submerged-membrane tank of the SMHS.

Coagulation pretreatment removed most of the NOM, but it did not influence competitive adsorption of MIB and NOM. Consequently, the concentration of the EBC was almost the same before and after coagulation pretreatment, which indicates that the EBC was not removed by coagulation. However, the intraparticle diffusivity of MIB in AC decreased significantly with time in coagulant-treated NOM water.

Acknowledgements

This study was supported by a Grant-in-Aid for Scientific Research S (no. 16H06362) and A (no. 21H04567) and a Grant-in-Aid for Scientific Research Activity Start-up (no. 20K22425) from the Japan Society for the Promotion of Science.

References

645 Akaike, H. 1974. A new look at the statistical model identification. IEEE Transactions on Automatic
646 Control 19(6), 716-723.
647 Altmann, J., Zietzschmann, F., Geiling, E.-L., Ruhl, A.S., Sperlich, A. and Jekel, M. 2015. Impacts of
648 coagulation on the adsorption of organic micropollutants onto powdered activated carbon in
649 treated domestic wastewater. Chemosphere 125, 198-204.
650 Amaral, P., Partlan, E., Li, M., Lapolli, F., Mefford, O.T., Karanfil, T. and Ladner, D.A. 2016. Superfine
651 powdered activated carbon (S-PAC) coatings on microfiltration membranes: Effects of milling
652 time on contaminant removal and flux. Water Research 100, 429-438.
653 Aschermann, G., Neubert, L., Zietzschmann, F. and Jekel, M. 2019a. Impact of different DOM size
654 fractions on the desorption of organic micropollutants from activated carbon. Water research
655 161, 161-170.
656 Aschermann, G., Schröder, C., Zietzschmann, F. and Jekel, M. 2019b. Organic micropollutant desorption
657 in various water matrices-Activated carbon pore characteristics determine the reversibility of
658 adsorption. Chemosphere 237, 124415.
659 Aschermann, G., Zietzschmann, F. and Jekel, M. 2018. Influence of dissolved organic matter and
660 activated carbon pore characteristics on organic micropollutant desorption. Water research
661 133, 123-131.
662 Banat, F.A., Al-Bashir, B., Al-Asheh, S. and Hayajneh, O. 2000. Adsorption of phenol by bentonite.
663 Environmental Pollution 107(3), 391-398.
664 Burnham, K.P. and Anderson, D.R. (2002) Model selection and multi-model inference A Practical
665 Information-Theoretic Approach, Springer.
666 Campinas, M. and Rosa, M.J. 2010. Removal of microcystins by PAC/UF. Separation and Purification
667 Technology 71(1), 114-120.
668 Campos, C., Marinas, B.J., Snoeyink, V.L., Baudin, I. and Laine, J.M. 2000a. PAC-membrane filtration
669 process. I: Model development. Journal of environmental engineering 126(2), 97-103.
670 Campos, C., Marinas, B.J., Snoeyink, V.L., Baudin, I. and Laine, J.M. 2000b. PAC-membrane filtration
671 process. II: Model application. Journal of environmental engineering 126(2), 104-111.
672 Chen, Y., Nakazawa, Y., Matsui, Y., Shirasaki, N. and Matsushita, T. 2020. Sulfate ion in raw water affects
673 performance of high-basicity PACl coagulants produced by Al (OH) 3 dissolution and base-
674 titration: Removal of SPAC particles by coagulation-flocculation, sedimentation, and sand
675 filtration. Water Research 183, 116093.
676 Chern, J.-M. and Wu, C.-Y. 2001. Desorption of dye from activated carbon beds: effects of temperature,
677 pH, and alcohol. Water Research 35(17), 4159-4165.
678 Corwin, C.J. and Summers, R.S. 2011. Adsorption and desorption of trace organic contaminants from
679 granular activated carbon adsorbers after intermittent loading and throughout backwash
680 cycles. Water research 45(2), 417-426.
681 Crittenden, J.C., Luft, P. and Hand, D.W. 1985. Prediction of multicomponent adsorption equilibria in
682 background mixtures of unknown composition. Water Research 19(12), 1537-1548.

683 Edzwald, J.K. (2010) Water Quality and Treatment A Handbook on Drinking Water, McGrawHill.
684 Gillogly, T.E.T., Snoeyink, V.L., Newcombe, G. and Elarde, J.R. 1999. A simplified method to determine
685 the powdered activated carbon dose required to remove methylisoborneol. Water Science and
686 Technology 40(6), 59-64.
687 Graham, M.R., Summers, R.S., Simpson, M.R. and MacLeod, B.W. 2000. Modeling equilibrium
688 adsorption of 2-methylisoborneol and geosmin in natural waters. Water Research 34(8), 2291-
689 2300.
690 Hand, D.W., Loper, S., Ari, M. and Crittenden, J.C. 1985. Prediction of multicomponent adsorption
691 equilibria using ideal adsorbed solution theory. Environmental science & technology 19(11),
692 1037-1043.
693 Hepplewhite, C., Newcombe, G. and Knappe, D. 2004. NOM and MIB, who wins in the competition for
694 activated carbon adsorption sites? Water Science and Technology 49(9), 257-265.
695 Ho, L. and Newcombe, G. 2005. Effect of NOM, turbidity and floc size on the PAC adsorption of MIB
696 during alum coagulation. Water Research 39(15), 3668-3674.
697 Kilduff, J.E. and Karanfil 1998. TCE adsorption by GAC preloaded with humic substances. Journal -
698 American Water Works Association 90(5), 76.
699 Kim, H.-S., Takizawa, S. and Ohgaki, S. 2007. Application of microfiltration systems coupled with
700 powdered activated carbon to river water treatment. Desalination 202(1-3), 271-277.
701 Kim, J.S., Lee, S.J., Yoon, S.H. and Lee, C.H. 1996. Competitive adsorption of trace organics on
702 membranes and powdered activated carbon in powdered activated carbon-ultrafiltration
703 system. Water Science and Technology 34(9), 223-229.
704 Knappe, D.R.U., Matsui, Y., Snoeyink, V.L., Roche, P., Prados, M.J. and Bourbigot, M.-M. 1998. Predicting
705 the Capacity of Powdered Activated Carbon for Trace Organic Compounds in Natural Waters.
706 Environmental Science & Technology 32(11), 1694-1698.
707 Lee, J.-W., Choi, S.-P., Thiruvenkatachari, R., Shim, W.-G. and Moon, H. 2006. Submerged microfiltration
708 membrane coupled with alum coagulation/powdered activated carbon adsorption for
709 complete decolorization of reactive dyes. Water Research 40(3), 435-444.
710 Li, L., Yang, S., Yu, S. and Zhang, Y. 2019. Variation and removal of 2-MIB in full-scale treatment plants
711 with source water from Lake Tai, China. Water Research 162, 180-189.
712 Li, Q., Mariñas, B.J., Snoeyink, V.L. and Campos, C. 2003. Three-component competitive adsorption
713 model for flow-through PAC systems. 2. Model application to a PAC/membrane system.
714 Environmental science & technology 37(13), 3005-3011.
715 Liu, H., Pan, D., Zhu, M. and Zhang, D. 2016. Occurrence and Emergency Response of 2-
716 Methylisoborneol and Geosmin in a Large Shallow Drinking Water Reservoir. CLEAN – Soil, Air,
717 Water 44(1), 63-71.
718 Loo, S.-L., Fane, A.G., Krantz, W.B. and Lim, T.-T. 2012. Emergency water supply: A review of potential
719 technologies and selection criteria. Water Research 46(10), 3125-3151.
720 Löwenberg, J., Zenker, A., Baggenstos, M., Koch, G., Kazner, C. and Wintgens, T. 2014. Comparison of

721 two PAC/UF processes for the removal of micropollutants from wastewater treatment plant
722 effluent: Process performance and removal efficiency. Water Research 56, 26-36.
723 Martin, E., Lalley, J., Wang, W., Nadagouda, M.N., Sahle-Demessie, E. and Chae, S.-R. 2018. Phosphate
724 recovery from water using cellulose enhanced magnesium carbonate pellets: Kinetics,
725 isotherms, and desorption. Chemical Engineering Journal 352, 612-624.
726 Masakazu, Y. 1988. Musty Odour Problems in Lake Biwa 1982-1987. Water Science and Technology
727 20(8-9), 133-142.
728 Matsui, Y., Aizawa, T., Kanda, F., Nigorikawa, N., Mima, S. and Kawase, Y. 2007. Adsorptive removal of
729 geosmin by ceramic membrane filtration with super-powdered activated carbon. Journal of
730 Water Supply: Research & Technology-AQUA 56.
731 Matsui, Y., Ando, N., Sasaki, H., Matsushita, T. and Ohno, K. 2009a. Branched pore kinetic model analysis
732 of geosmin adsorption on super-powdered activated carbon. Water Research 43(12), 3095-
733 3103.
734 Matsui, Y., Fukuda, Y., Inoue, T. and Matsushita, T. 2003. Effect of natural organic matter on powdered
735 activated carbon adsorption of trace contaminants: characteristics and mechanism of
736 competitive adsorption. Water Research 37(18), 4413-4424.
737 Matsui, Y., Hasegawa, H., Ohno, K., Matsushita, T., Mima, S., Kawase, Y. and Aizawa, T. 2009b. Effects of
738 super-powdered activated carbon pretreatment on coagulation and trans-membrane pressure
739 buildup during microfiltration. Water Research 43(20), 5160-5170.
740 Matsui, Y., Nakao, S., Sakamoto, A., Taniguchi, T., Pan, L., Matsushita, T. and Shirasaki, N. 2015.
741 Adsorption capacities of activated carbons for geosmin and 2-methylisoborneol vary with
742 activated carbon particle size: Effects of adsorbent and adsorbate characteristics. Water
743 Research 85, 95-102.
744 Matsui, Y., Nakao, S., Taniguchi, T. and Matsushita, T. 2013. Geosmin and 2-methylisoborneol removal
745 using superfine powdered activated carbon: Shell adsorption and branched-pore kinetic model
746 analysis and optimal particle size. Water research 47(8), 2873-2880.
747 Matsui, Y., Yoshida, T., Nakao, S., Knappe, D.R.U. and Matsushita, T. 2012. Characteristics of competitive
748 adsorption between 2-methylisoborneol and natural organic matter on superfine and
749 conventionally sized powdered activated carbons. Water Research 46(15), 4741-4749.
750 Matsui, Y., Yuasa, A. and Ariga, K. 2001. Removal of a synthetic organic chemical by PAC-UF systems—
751 I: theory and modeling. Water Research 35(2), 455-463.
752 Najm, I.N., Snoeyink, V.L. and Richard, Y. 1991. Effect of Initial Concentration of a SOC in Natural Water
753 on Its Adsorption by Activated Carbon. Journal - American Water Works Association 83(8), 57-
754 63.
755 Nakayama, A., Sakamoto, A., Matsushita, T., Matsui, Y. and Shirasaki, N. 2020. Effects of pre, post, and
756 simultaneous loading of natural organic matter on 2-methylisoborneol adsorption on superfine
757 powdered activated carbon: Reversibility and external pore-blocking. Water Research 182,
758 115992.

759 Newcombe, G., Drikas, M. and Hayes, R. 1997. Influence of characterised natural organic material on
760 activated carbon adsorption: II. Effect on pore volume distribution and adsorption of 2-
761 methylisoborneol. Water Research 31(5), 1065-1073.
762 Newcombe, G., Morrison, J., Hepplewhite, C. and Knappe, D.R.U. 2002. Simultaneous adsorption of
763 MIB and NOM onto activated carbon: II. Competitive effects. Carbon 40(12), 2147-2156.
764 Ocampo-Pérez, R., Abdel daiem, M.M., Rivera-Utrilla, J., Méndez-Díaz, J.D. and Sánchez-Polo, M. 2012.
765 Modeling adsorption rate of organic micropollutants present in landfill leachates onto granular
766 activated carbon. Journal of Colloid and Interface Science 385(1), 174-182.
767 Pan, L., Matsui, Y., Matsushita, T. and Shirasaki, N. 2016. Superiority of wet-milled over dry-milled
768 superfine powdered activated carbon for adsorptive 2-methylisoborneol removal. Water
769 Research 102, 516-523.
770 Peel, R.G., Benedek, A. and Crowe, C.M. 1981. A branched pore kinetic model for activated carbon
771 adsorption. AIChE Journal 27(1), 26-32.
772 Qi, S., Schideman, L., Mariñas, B.J., Snoeyink, V.L. and Campos, C. 2007. Simplification of the IAST for
773 activated carbon adsorption of trace organic compounds from natural water. Water Research
774 41(2), 440-448.
775 Schideman, L., Snoeyink, V., Marinas, B.J. and Kosterman, M. 2002. Pilot plant study on the
776 performance and optimization of submerged membranes for taste and odor removal. Water
777 Science and Technology: Water Supply 2(2), 185-192.
778 Schwarz, G. 1978. Estimating the Dimension of a Model. Ann. Statist. 6(2), 461-464.
779 Shanmuganathan, S., Loganathan, P., Kazner, C., Johir, M.A.H. and Vigneswaran, S. 2017. Submerged
780 membrane filtration adsorption hybrid system for the removal of organic micropollutants from
781 a water reclamation plant reverse osmosis concentrate. Desalination 401, 134-141.
782 Sidney Seckler, F.F., Margarida, M. and Rosemeire, A.L. 2013. Interference of iron as a coagulant on MIB
783 removal by powdered activated carbon adsorption for low turbidity waters. Journal of
784 Environmental Sciences 25(8), 1575-1582.
785 Sillanpää, M. (2014) Natural organic matter in water: Characterization and treatment methods,
786 Butterworth-Heinemann.
787 Singh, R. (2005) Hybrid membrane systems – applications and case studies, Elsevier Science, Amsterdam.
788 Sontheimer, H., Crittenden, J.C., Summers, R.S., Hubele, C., Roberts, C. and Snoeyink, V.L. (1988)
789 Activated carbon for water treatment, DVGW-Forschungsstelle, Engler-Bunte-Institut,
790 Universitaet Karlsruhe (TH), Karlsruhe.
791 Stoquart, C., Servais, P. and Barbeau, B. 2014. Ammonia removal in the carbon contactor of a hybrid
792 membrane process. Water Research 67, 255-266.
793 Stoquart, C., Servais, P., Bérubé, P.R. and Barbeau, B. 2012. Hybrid Membrane Processes using activated
794 carbon treatment for drinking water: A review. Journal of Membrane Science 411-412, 1-12.
795 Suzuki, M. (1990) Adsorption engineering, Kodansha Tokyo.
796 Takahashi, T., Takase, K., Takeshita, K., Kawano, H., Mamizuka, M. and Kizu, H.J.J.o.J.S.o.W.E. 2016. State

797 transition of musty-odor-producing cyanobacteria and 2-methylisoborneol in the Serikawa
798 dam reservoir. Journal of Japan Society on Water Environment 39(2), 51-62.
799 Tansakul, C., Laborie, S. and Cabassud, C. 2011. Adsorption combined with ultrafiltration to remove
800 organic matter from seawater. Water Res 45(19), 6362-6370.
801 To, P.C., Mariñas, B.J., Snoeyink, V.L. and Ng, W.J. 2008a. Effect of pore-blocking background compounds
802 on the kinetics of trace organic contaminant desorption from activated carbon. Environmental
803 science & technology 42(13), 4825-4830.
804 To, P.C., Mariñas, B.J., Snoeyink, V.L. and Ng, W.J. 2008b. Effect of strongly competing background
805 compounds on the kinetics of trace organic contaminant desorption from activated carbon.
806 Environmental science & technology 42(7), 2606-2611.
807 Villadsen, J.V. and Stewart, W.E. 1967. Solution of boundary-value problems by orthogonal collocation.
808 Chemical Engineering Science 22(11), 1483-1501.
809 Xing, J., Liang, H., Xu, S., Chuah, C.J., Luo, X., Wang, T., Wang, J., Li, G. and Snyder, S.A. 2019. Organic
810 matter removal and membrane fouling mitigation during algae-rich surface water treatment
811 by powdered activated carbon adsorption pretreatment: Enhanced by UV and UV/chlorine
812 oxidation. Water Research 159, 283-293.
813 Yan, M., Wang, D., Ni, J., Qu, J., Chow, C.W.K. and Liu, H. 2008. Mechanism of natural organic matter
814 removal by polyaluminum chloride: Effect of coagulant particle size and hydrolysis kinetics.
815 Water Research 42(13), 3361-3370.
816 Yuan, J., Huang, Y., Nie, Z. and Hofmann, R. 2020. The effect of water temperature on the removal of
817 2-methylisoborneol and geosmin by preloaded granular activated carbon. Water Research 183,
818 116065.
819

Supplementary Information

Desorption of micropollutant from superfine and normal powdered activated carbon in submerged-membrane system due to influent concentration change in the presence of natural organic matter: experiments and two-component branched-pore kinetic model

Long Pan [a], Akiko Nakayama [b], Yoshihiko Matsui [a*], Taku Matsushita [a], and Nobutaka Shirasaki [a]

[a] Faculty of Engineering, Hokkaido University, N13W8, Sapporo 060-8628, Japan

[b] Graduate School of Engineering, Hokkaido University, N13W8, Sapporo 060-8628, Japan

* Corresponding author. Tel/fax: +81-11-706-7280

E-mail address: matsui@eng.hokudai.ac.jp

1. Analytical method of MIB

MIB concentrations were determined with a gas chromatograph–mass spectrometer (7820A/5977 E MSD, Agilent, which was coupled to a headspace solid-phase microextraction system (PAL RSI 85, Agilent Technologies Japan, Tokyo, Japan) assembled with a Carboxen®/PDMS fiber (85 µm, Stableflex™, 24 Ga, Agilent). All the regents were obtained from Wako Pure Chemical Industries, Osaka, Japan. The sampled solution was filtered through a 0.2-µm PTFE membrane ((DISMIC-25HP; Toyo Roshi Kaisha, Ltd., Tokyo), dosed with 2,4,6-trichloroanisole-d_3 as the internal standard and oversaturated with NaCl. The pretreated solution was incubated at 80 °C for 5 min and gas-phase was extracted for 30 min by the fiber which went through 300 °C conditioning each time. The extracted sample was desorbed and released to gas chromatograph and carried by 1.5 mL/min He gas under 15:1 split mode through a HP-5MS column (30 m * 250 µm * 0.25 µm) with 50 °C (hold for 5 min) -140 °C (60 °C/min) – 160 °C (5 °C/min) – 280 °C (60 °C/min, hold for 2 min). The temperature of ion source and quadrupole in the mass spectrometer were 230 °C and 150 °C respectively. The retention time of MIB and internal standard went to 3.59 min and 4.37 min. MIB concentrations were determined by monitoring for MIB (*m/z* 95 referenced by *m/z* 108) and the internal standard (*m/z* 195 referenced by *m/z* 167). The limit of detection is 5 ng/L while the limit of quantification is 10 ng/L.

2. Adsorption-desorption model for the SMHS-PAC/SPAC

Nomenclature

i, adsorbate *i* (MIB or EBC)
$C_i(t)$, concentration of adsorbate *i* in the effluent of the SMHS-PAC/SPAC (nmol/cm^3 = µmol/L) at time *t*
$C_{\mathrm{IN},i}$, concentration of adsorbate *i* in the influent of the SMHS-PAC/SPAC (nmol/cm^3 = µmol/L)
$c_{\mathrm{M},i}(t,r)$, liquid-phase concentration in the macropores of an AC particle at radial distance *r* and time *t* (nmol/cm^3 = µmol/L)
$D_{\mathrm{P},i}$, diffusion coefficient in macropores (cm^2/s)
$D_{\mathrm{M},i}$, diffusity in water (cm^2/s)
$k_{\mathrm{f},i}$, external mass transfer coefficient (cm/s)
$k_{\mathrm{S},i}$, mass transfer rate coefficient in micropores (s^{-1})
$K_{\mathrm{LA},i}$, rate constant for loss due to volatilization (s^{-1})
$K_{\mathrm{F},i}$, Freundlich constant $\left[(\mathrm{nmol/mg})/(\mathrm{nmol/cm^3})^{1/n_{\mathrm{F},i}} = (\mathrm{\mu mol/g})/(\mathrm{\mu mol/L})^{1/n_{\mathrm{F},i}}\right]$
$n_{\mathrm{F},i}$, Freundlich exponent (dimensionless)
$q_i(t,r)$, solid-phase concentration (adsorbate loading per gram of AC) at radial distance *r* and time *t*, which is given by equation (1) (nmol/mg = µmol/g)
$q_{\mathrm{M},i}(t,r)$, adsorbate loading per gram of AC around macropore at radial distance *r* and time *t* (nmol/mg = µmol/g)
$q_{\mathrm{B},i}(t,r)$, adsorbate loading per gram of AC around micropore at radial distance *r* and time *t* (nmol/mg = µmol/g)
r, radial distance from the center of an AC particle (cm)
R, AC particle radius (cm)
t, time (s)

$C_{0,\mathrm{MIB}}$, initial concentration of MIB in a batch adsorption experiment (nmol/cm^3 = µmol/L)
$C_{0,\mathrm{EBC}}$, initial concentration of an EBC in a batch adsorption experiment (nmol/cm^3 = µmol/L)
$C_{\mathrm{E,MIB}}$, equilibrium liquid-phase concentration of MIB (nmol/cm^3 = µmol/L)
$C_{\mathrm{E,EBC}}$, equilibrium liquid-phase concentration of equivalent background compound (EBC) (nmol/cm^3 = µmol/L)
C_{C}, AC dose (mg/cm^3 = g/L)

N, number of adsorbates (dimensionless)
Q, flow rate (cm^3/s)
$q_{E,MIB}$, equilibrium solid-phase concentration of MIB (nmol/mg = μmol/g)
$q_{E,EBC}$, equilibrium solid-phase concentration of EBC (nmol/mg = μmol/g)
V, volume of the submerged-membrane tank (cm^3)
ε, AC porosity (dimensionless)
ρ, AC particle density (mg/cm^3)
$\emptyset$, fraction of total adsorptive capacity available in macropores (dimensionless)
τ, tortuosity defined as the ratio of actual diffusion path length of a molecule to the shortest distance of its straight line (dimensionless)
n, number of experimental points for fitting
m, number of fitting parameters
AIC, Akaike information criterion
BIC, Bayesian information criterion
MSD, mean squared deviation

2.1. Development of a model for multicomponent adsorption-desorption kinetics in the submerged-membrane tank

We constructed a multicomponent model for the kinetics of adsorption-desorption of MIB molecules on the PAC/SPAC in the SMHS by using the BPKM of Peel et al. (1981). The BPKM divides carbon particle into two regions of different diffusion rates, which are loosely termed macropores and micropores (note: these terms should not be confused with their conventional uses to define certain pore size ranges). The BPKM consisted of three mass transfer resistances in series (Fig. 3S): passage of adsorbates across the external surface of an AC particle, intraparticle diffusion of the adsorbates in the macropores, and mass transfer from the macropore to the micropores.

Since the parts of the total adsorptive capacity which are utilized in macropores and micropores are $\emptyset$ and $(1-\emptyset)$, respectively, the adsorbate loading per gram of AC (solid phase concentration) is given by:

$$q_i(t,r) = \emptyset q_{\mathrm{M},i}(t,r) + (1-\emptyset) \times q_{\mathrm{B},i}(t,r) \qquad (1S)$$

Here, it was assumed that the macropores and micropores are uniformly distributed throughout the particles (Peel et al., 1981). Therefore, $\emptyset$ is not a function of the radial direction, but is treated as a constant value.

The mass transfer rate for an adsorbate from macropore to micropores is described by a linear driving force model based on the solid-phase concentration difference (Peel et al., 1981). The mass balance in micropore is as follows:

$$\frac{\partial q_{\mathrm{B},i}(t,r)}{\partial t} = \frac{k_{\mathrm{S},i}}{1-\emptyset}\left[q_{\mathrm{M},i}(t,r) - q_{\mathrm{B},i}(t,r)\right] \qquad (2S)$$

By assuming that radial mass transport in an AC particle occurs by pore diffusion in the liquid phase of macropores, the mass balance equation in macropores is as follows:

$$\frac{\partial q_{\mathrm{M},i}(t,r)}{\partial t} = \frac{\varepsilon D_{\mathrm{P,i}}}{\rho r^2}\frac{\partial}{\partial r}\left[r^2\frac{\partial c_{\mathrm{M,i}}(t,r)}{\partial r}\right] - \frac{k_{\mathrm{S},i}}{\emptyset}\left[q_{\mathrm{M},i}(t,r) - q_{\mathrm{B},i}(t,r)\right] \qquad (3S)$$

Here, the adsorbate in the liquid phase of the macro-pores is not incorporated in the equation for the simplicity because it is negligibly small compared to the adsorbed mass (Sontheimer et al., 1988).

The mass balance of an adsorbate *i* on an AC particle is described by equating the rate of the change

in adsorbate mass in the particle and adsorbate mass transfer from the external particle surface to the particle interior:

$$\frac{\mathrm{d}}{\mathrm{d}t}\left\{\int_0^R q_i(t,r)r^2\mathrm{d}r\right\} = \frac{k_{\mathrm{f},i}R^2}{\rho}\left[C_i(t) - c_{\mathrm{M},i}(t,R)\right] \qquad (4S)$$

A CSTR (continuous stirred tank reactor) model is applied to describe the mass balance equation for an adsorbate in a membrane tank.

$$\frac{\mathrm{d}C_i(t)}{\mathrm{d}t} = -\frac{3C_{\mathrm{C}}k_{\mathrm{f},i}}{\rho R}\left[C_i(t) - c_{\mathrm{M},i}(t,R)\right] + C_{\mathrm{IN},i}\frac{Q}{V} - C_i(t)\frac{Q}{V} - K_{\mathrm{LA},i}C_i(t) \qquad (5S)$$

Local adsorption equilibrium between the liquid phase and the pore surface in the macropores of an AC particle is assumed, and the equilibrium is expressed by the IAST (ideal adsorption solution theory)–Freundlich isotherm equation (Crittenden et al., 1985; Hand et al., 1985) :

$$c_{\mathrm{M,i}}(t,r) = \frac{q_{\mathrm{M,i}}(t,r)}{\sum_{j=1}^{N} q_{\mathrm{M,j}}(t,r)}\left[\frac{\sum_{j=1}^{N} n_{\mathrm{F},i}q_{\mathrm{M,j}}(t,r)}{n_{\mathrm{F},i}K_{\mathrm{F},i}}\right]^{n_{\mathrm{F},i}} \qquad (6S)$$

It should be noted that the use of the adsorption equilibrium equation implicitly assumes that adsorption is reversible, that is, that 100% desorption occurs when the liquid-phase concentration goes to zero.

Intra-particle coefficient ($D_{\mathrm{P,i}}$) equals diffusivity in water ($D_{\mathrm{M,i}}$) divided by tortuosity (τ).

$$D_{\mathrm{P,i}} = D_{\mathrm{M,i}}/\tau \qquad (7S)$$

Equation (3S) was converted to one-dimensional differential equations with respect to time *t* by means of the orthogonal collocation (Villadsen and Stewart, 1967). The converted equation and other equations were solved as a system of ordinary differential equations by the Gear's BDF (backward differentiation formula) method in the International Mathematics and Statistics Library (IMSL) software collection.

2.2. Conversion of equations 1–5 in the main manuscript to ordinary differential equations

$\boldsymbol{B}_{n,k}^{\mathrm{T}}$ is the Laplacian operator matrix, $\boldsymbol{W}_j^{\mathrm{T}}$ is the integral operator vector of the orthogonal collocation method, and N_{C} is the number of collocation points ($N_{\mathrm{C}} = 24$ in the numerical calculations carried out in this study).

$$\emptyset\frac{dq_{\mathrm{M},i,n}(t)}{dt} = \frac{D_{\mathrm{P},i}}{\rho R^2}\sum_{k=1}^{N_{\mathrm{C}}}\boldsymbol{B}_{n,k}^{\mathrm{T}}\frac{q_{\mathrm{M},i,k}(t)}{\sum_{j=1}^{N} q_{\mathrm{M},j,k}(t)}\left[\frac{\sum_{j=1}^{N} n_{\mathrm{F},j}q_{\mathrm{M},j,k}(t)}{n_{\mathrm{F},i}K_{F,i}}\right]^{n_{\mathrm{F},i}} - k_{\mathrm{B},i}\left[q_{\mathrm{M},i,n}(t) - q_{\mathrm{B},i,n}(t)\right]$$
$$n = 1, N_{\mathrm{C}} - 1 \qquad (8S)$$

$$\begin{aligned}
&\emptyset\frac{dq_{\mathrm{M},i,N_{\mathrm{C}}}(t)}{dt} \\
&= \frac{k_{f,i}}{\boldsymbol{W}_{N_{\mathrm{C}}}^{\mathrm{T}}\rho R_m}\left\{C_i(t) - \frac{q_{\mathrm{M},i,N_{\mathrm{C}}}(t)}{\sum_{j=1}^{N} q_{\mathrm{M},j,N_{\mathrm{C}}}(t)}\left[\frac{\sum_{j=1}^{N} n_{\mathrm{F},j}q_{\mathrm{M},j,N_{\mathrm{C}}}(t)}{n_{\mathrm{F},i}K_{\mathrm{F},i}}\right]^{n_{\mathrm{F},i}}\right\} - k_{\mathrm{B},i}\left[q_{\mathrm{M},i,N_{\mathrm{C}}}(t) - q_{\mathrm{B,i},N_{\mathrm{C}}}(t)\right] \\
&\quad - \sum_{j=1}^{N_{\mathrm{C}}-1}\left\langle\frac{\boldsymbol{W}_j^{\mathrm{T}}}{\boldsymbol{W}_{N_{\mathrm{C}}}^{\mathrm{T}}}\left\{\frac{D_{\mathrm{P},i}}{\rho R^2}\sum_{k=1}^{N_{\mathrm{C}}}\boldsymbol{B}_{j,k}^{\mathrm{T}}\frac{q_{\mathrm{M},i,k}(t)}{\sum_{j=1}^{N} q_{\mathrm{M},j,k}(t)}\left[\frac{\sum_{j=1}^{N} n_{\mathrm{F},j}q_{\mathrm{M},j,k}(t)}{n_{\mathrm{F},i}K_{\mathrm{F},i}}\right]^{n_{\mathrm{F},i}}\right\}\right\rangle
\end{aligned}$$

(9S)

$$(1-\emptyset)\frac{dq_{\mathrm{B},i,n}(t)}{dt} = k_{\mathrm{B},i}\left[q_{\mathrm{M},i,n}(t) - q_{\mathrm{B},i,n}(t)\right] \qquad n = 1, N_{\mathrm{C}} \tag{10S}$$

$$\frac{dC_i(t)}{dt} = -\frac{3C_{\mathrm{C}}k_{f,i}}{\rho R}\left\{C_i(t) - \frac{q_{\mathrm{M},i,N_C}(t)}{\sum_{j=1}^{N} q_{\mathrm{M},j,N_C}(t)}\left[\frac{\sum_{j=1}^{N} n_{\mathrm{F},j}q_{\mathrm{M},j,N_{\mathrm{C}}}(t)}{n_{\mathrm{F},i}K_{\mathrm{F},i}}\right]^{n_{\mathrm{F},i}}\right\} + \left[C_{\mathrm{IN},i} - C_i(t)\right]\frac{Q}{V} - K_{\mathrm{LA},i}C_i(t) \tag{11S}$$

2.3. Isotherm parameter estimation method

To describe competitive adsorption of background NOM and MIB, we used an equivalent background compound (EBC) method (Graham et al., 2000; Najm et al., 1991; Newcombe et al., 2002), where the EBC is a hypothetical compound that represents NOM that competes with the target compound (MIB in this research) for adsorption sites. Thus, equation (6S) becomes two equations for the two-component system comprising MIB and EBC:

$$C_{\mathrm{E,MIB}} = \frac{q_{\mathrm{E,MIB}}}{q_{E,\mathrm{MIB}} + q_{\mathrm{E,EBC}}}\left(\frac{q_{\mathrm{E,MIB}}\, n_{\mathrm{F,MIB}} + q_{\mathrm{E,EBC}}\, n_{\mathrm{F,EBC}}}{K_{\mathrm{F,MIB}}\, n_{\mathrm{F,MIB}}}\right)^{n_{\mathrm{F,MIB}}} \tag{12S}$$

$$C_{\mathrm{E,EBC}} = \frac{q_{\mathrm{E,EBC}}}{q_{\mathrm{E,MIB}} + q_{\mathrm{E,EBC}}}\left(\frac{q_{\mathrm{E,MIB}}\, n_{\mathrm{F,MIB}} + q_{\mathrm{E,EBC}}\, n_{\mathrm{F,EBC}}}{K_{\mathrm{F,EBC}}\, n_{\mathrm{F,EBC}}}\right)^{n_{\mathrm{F,EBC}}} \tag{13S}$$

The mass balance in a vial used for batch adsorption experiments was as follows:

$$C_{\mathrm{E,MIB}} = C_{0,\mathrm{MIB}} - q_{\mathrm{E,MIB}}\, C_{\mathrm{C}} \tag{14S}$$

$$C_{\mathrm{E,EBC}} = C_{0,\mathrm{EBC}} - q_{\mathrm{E,EBC}}\, C_{\mathrm{C}} \tag{15S}$$

Once the initial concentrations and the Freundlich constants and exponents for MIB and EBC are known, the MIB concentration for each AC dosage can be calculated by solving equations (12S)–(15S). In the EBC method, the equations are repeatedly solved by assuming those for EBC ($C_{0,\mathrm{EBC}}$, $K_{\mathrm{F,EBC}}$, and $n_{\mathrm{F,EBC}}$) to search for the best fit of the calculated MIB concentrations to the experimentally observed concentrations. In this study, we conducted searches to minimize the *MSD*, which corresponds to the average of relative squared errors between the observed and calculated concentrations, by applying a modified Levenberg–Marquardt algorithm from the IMSL.

3. Parameter value evaluation for adsorption isotherm

The EBC method for fitting the isotherm of a micropollutant in the presence of NOM typically involves a search for three parameter values: the initial liquid-phase concentration ($C_{0,EBC}$), the Freundlich constant ($K_{F,EBC}$), and the Freundlich exponent ($n_{F,EBC}$) of the EBC (NOM) (Najm et al., 1991). However, determining unique values for $K_{F,EBC}$ and $n_{F,EBC}$ is often difficult (Graham et al., 2000; Knappe et al., 1998; Najm et al., 1991; Qi et al., 2007). Therefore, we used the EBC method under three conditions (A–C) Table 2): (A) we searched for all three parameter values (the conventional EBC method), (B) we searched only for $C_{0,EBC}$ and $n_{F,EBC}$ values on the assumption that $K_{F,EBC} = K_{F,MIB}$, and (C) we searched only for the $C_{0,EBC}$ value on the assumptions that $K_{F,EBC} = K_{F,MIB}$ and $n_{F,MIB} = n_{F,EBC}$. The assumptions used for conditions B and C were based on the fact that the characteristics of NOM (the EBC), including its molecular weight, were similar to those of the target adsorbate, MIB (Hepplewhite et al., 2004; Kilduff and Karanfil, 1998; Matsui et al., 2012; Newcombe et al., 1997; Newcombe et al., 2002). We evaluated the data fit by using Akaikes information criterion (*AIC*) and the Bayesian information criterion (*BIC*) (Akaike, 1974; Burnham and Anderson, 2002; Schwarz, 1978), which can evaluate overfitting/underfitting and which enable parameter selection.

$$AIC = n\ln(MSD) + 2m \qquad (16S)$$

$$BIC = n\ln(MSD) + m\ln(n) \qquad (17S)$$

The *AIC* and *BIC* values indicated that the most reasonable isotherm fitting was achieved under condition C, that is, by searching $C_{0,EBC}$ while fixing the Freundlich parameters of EBC to those of MIB (Table 2). The isotherm fits were also visually confirmed (Fig. 9S). The assumption that $K_{F,EBC}$ and $n_{F,EBC}$ were the same as $K_{F,MIB}$ and $n_{F,MIB}$, respectively, was appropriate because the values obtained for EBC under conditions A and B were similar to the MIB values.

The fact that the best fit was obtained under condition C indicates that some of the NOM, that is, NOM with adsorptive affinity similar to that of MIB, competed with MIB for adsorption. The estimated EBC concentration (0.223 μmol/L) was much higher than the MIB concentration (0.006 μmol/L) and was lower than the total NOM concentration (~ 3.2 mg/L, Table 2S); these results are consistent with the fact that the EBC concentration is generally much higher than the target micropollutant (MIB) concentration and that the EBC constitutes only a portion of NOM (Edzwald, 2010; Knappe et al., 1998; Matsui et al., 2003). EBC concentration was almost the same between the MIB-spiked NOM-water and the Coagulated MIB-spiked NOM-water, 0.247 μmol/L and 0.223 μmol/L, respectively, which clearly indicates that little EBC was removed by coagulation, as inferred from section 3.2.1.

4. Model simulation of the kinetics of adsorption-desorption in the SMHS-PAC/SPAC

Some of the parameters required for the BPKM simulation were predetermined from experiments independent of the SMHS experiments or from literatures. These parameters and the methods by which they were determined are presented in Table 5S. As mentioned in section 3.2.2, we assumed that the EBC molecule was similar in size to MIB and thus that the external mass transfer coefficients, pore diffusion coefficients, and micropore mass transfer coefficients were the same for MIB and EBC.

Finally, five unknown parameters remained. For these five parameters, we evaluated seven different search settings, and the parameter values were optimized for each setting (Table 3). With settings A and B, the model becomes the traditional intraparticle diffusion model, which is the simplest model and does not consider branched-pore diffusion. In contrast, settings C–G take branched-pore diffusion into account. The values of the unknown model parameters were determined by fitting the model simulations to the experimental data for the SMHS-PAC/SPAC with various AC dosages and various influent concentrations simultaneously. We evaluated the goodness of fit by means of a weighted *MSD* of the concentration according to the sampling-time interval, focusing on mass balance from the adsorption process to the desorption process. The search for optimized parameter

values with the best goodness of fit was conducted by means of a direct search complex algorithm method (BCPOL) and a quasi-Newton method (BCONF) in IMSL, starting from various initial guesses; in this way, the uniqueness of the optimized parameter values was confirmed.

The simulation results of the parameter search settings are summarized in Table 3. The simulation results obtained with setting A did not fit any of the experimental data (Fig. 10S). Even if the k_f values for PAC and SPAC were searched independently with setting B, the goodness of fit was still poor (Fig. 11S). These results imply that k_f did not influence the kinetics of MIB adsorption. For settings C (Fig. 12S) and D (Fig. 13S), which take into account branched-pore diffusion, the simulations fit the experimental data better, a result that is in accordance with previously reported research (Matsui et al., 2009). However, obvious discrepancies remained, particularly for the period from 0 to 6 h. These discrepancies were attributed to the change in intraparticle diffusivity due to the adsorption of NOM by the AC or to the effects of PACl, such as AC flocculation and hindrance of mass transfer/diffusivity by the aluminum precipitate (Ho and Newcombe, 2005; Sidney Seckler et al., 2013; To et al., 2008a, b).

With setting E (Fig. 14S), the pore diffusion coefficient (D_P) was assumed to change locally with the amount of adsorbed EBC: D_P decreases with increasing EBC loading at the location. Settings F (Fig. 6) and G (Fig. 15S) take into account the effects of NOM loading and/or coagulation in such a way that the pore diffusion coefficient or the external mass transfer coefficient, respectively, in an AC particle are assumed to decrease with the residence time of the AC in the SMHS. Because the temporal dependence of the diffusion coefficient was unknown in the settings, we divided the EBC loading or residence time into four/five intervals and estimated the diffusion coefficient for each interval. On the basis of the discussion of the previous paragraph, settings D and E also assume that external mass transfer was not the rate-determining step; specifically, a large k_f value (1.0 cm/s) was used, which decreased the number of search parameters. Of settings E–G, setting F gave the best fit to the experimental data with the smallest *MSD* value (Table 3). These results suggest that the decrease in uptake rate of MIB is related to the change in internal diffusion (D_P), not to the external mass transfer (k_f), and that the decrease in internal diffusion is not related to the amount of EBC adsorbed. The latter is consistent with previous findings that pore blockage is caused by large NOM molecules rather than small NOM molecules (To et al., 2008a, b). Compared with settings A–D, setting F has more parameters, so the better fit is not particularly surprising. Despite the larger number of parameters, preference should be given to setting F because it yielded the minimum values of both *AIC* and *BIC*.

Table 1S. Characteristics of the PAC (Taikou-W, Futamura Chemical Industries Co., Gifu, Japan)

Carbon	Median diameter (μm)	BET surface area (m^2/g)	pH_{pzc}
Taikou-W	18.9	1066	8.34
Ground Taikou-W	4.93	1269	7.66
	1.27	1208	7.54
	0.62	1130	7.72

The data is taken from the paper of (Matsui et al., 2015), in which the carbon is referred as Carbon-H.

Table 2S. Compositions of water samples.

	MIB	Na^+	K^+	SO_4^{2-}	NO^{3-}	Mg^{2+}	Ca^{2+}	HCO_3^-	Cl^-	DOC	NOM	UV absorbance at 260 nm	Figures
	µg/L	mg/L	mg/L	mg/L	mg/L	mg/L	mg/L	mg/L	mg/L	mg-C/L	mg/L	cm^{-1}	
NOM-free water	0	19.0	3.1	14.0	6.9	4.8	17.8	30.5	30.5	Not measured but very low			
MIB-spiked NOM-free water	1.18–1.37												5
Coagulated NOM-free water	0	NMSNF		NMHNF	NMSNF			NM	NMHNF				3, 4, 6-8, 2S, 6S, 8S, 10S-12S, 14S
NOM-water	0	12.2	1.3	15.2	0.2	3.9	5.4	8.2	11.1	2.52	4.85	0.09	-
MIB-spiked NOM-water	0.07–1.46												5, 4S
Coagulated NOM-water	0	11.8	1.3	16.1	0.2	3.8	4.9	NM	14.1	1.67	3.21	0.04	2-4, 6-8, 2S, 5S-8S, 10S-16S
Coagulated MIB-spiked NOM-water	0.08–1.17												All figures except 1S, 3S

All the water was adjusted to pH ~7.0.
The NOM concentrations are estimates from DOC with the assumption of carbon content 0.52 mg-C/mg (IHSS).
NM: not measured.
NMSNF: Not measured but similar to NOM-free water because the coagulant did not contain Na^+, K^+, NO^{3-}, Mg^{2+}, and Ca^{2+}.
NMHNF: Not measured but slightly higher than NOM-free water because the introductions via coagulant were theoretically less than 1.0 and 2.5 mg/L for SO_4^{2-} and Cl^-, respectively, according to the coagulant specification and dosage.
Ion concentrations, DOC, and the absorbance at 260 nm in the water were measured by an ion chromatography system (Integrion and ICS-1100; Thermo Scientific, Bremen, Germany), a TOC analyzer (TOC900; GE Analytical Instruments, Inc., Boulder, CO, USA), and a spectrophotometer (UV-1800; Shimadzu, Kyoto, Japan), respectively.

Table 3S. Configuration of the SMHS.

Component	Configuration	Related specification
Raw-water tank	5-L-capacity glass tank containing raw water	Constant outflow rate, 1.3 mL/min in each tube emanating from the tank
Coagulant tank	200-mL-capacity polypropylene tank containing the coagulant	Constant outflow rate, 0.12 mL/min in each tube emanating from the tank
Submerged-membrane tank	100-mL-capacity glass tank holding 65 mL of water Hydraulic retention time 46 min Set of membranes submerged in the water Magnetic stirrer bar (1000 rpm)	4 hollow-fiber PVDF membrane with a pore size of 0.1 μm (Asahi Kasei Corp., Tokyo, Japan), a length of 7 cm, and a closed tip Effective membrane surface area, 12 cm^2 Filtration flux, 0.069 m/h
Feeding line	Peristaltic pumps Glass tubes with small, short plastic connectors Static mixers	Limited use of plastic minimized MIB loss by sorption onto the plastic Coagulant and raw water were mixed by means of static mixers and were pumped to the submerged-membrane tank or to the blank sample collector
Effluent collector	Peristaltic pumps Glass tubes with small plastic connectors Glass bottles pretreated by heating at 550 °C	Membrane filtrate pumped out at a constant flow rate of 1.42 mL/min and fraction-collected into collectors

Table 4S. Mass balance of MIB in the SMHS-PAC/SPAC.

Designation	Contents	Condition
A	MIB adsorbed on AC	A = B + C – D – E – F
B	Initial MIB in the submerged-membrane tank	65 mL of solution containing ~1 μg/L ($C_{\mathrm{IN,MIB}}$) MIB at t = 0 h
C	Influent MIB	Influent containing ~1 μg/L ($C_{\mathrm{IN,MIB}}$) MIB; flow rate, 1.42 mL/min from 0 h to t
D	MIB remaining in the submerged-membrane tank	65 mL of solution containing MIB (C_{MIB}) at t
E	Effluent MIB	Effluent containing MIB (C_{MIB}); flow rate, 1.42 mL/min from 0 h to t
F	Volatilized MIB	Loss due to volatilization from 0 h to t; $K_{\mathrm{LA},i}$ = 4.84 × 10^{-5} s^{-1}

Table 5S. Input parameter values for adsorbent and adsorbate in the model.

Input parameter	SPAC	PAC
Median particle diameter, D_{50} (μm)	0.94	12.07
Apparent particle density, ρ (g/L)	850.0	
Porosity, ε (dimensionless)	0.53	
Diffusivity of MIB and EBC in water (cm^2/s)	6.46×10^{-6}	
Rate constant for MIB loss due to volatilization, $K_{LA,i}$ (s^{-1})	4.84×10^{-5}	
Effective HRT (min)	63.8 min	

AC particle size was determined with a laser-light-scattering instrument (Microtrac MT3300EXII, Nikkiso Co., Tokyo, Japan) after addition of a dispersant (Triton X-100, Kanto Chemical Co., Tokyo, Japan; final concentration, 0.08 vol %) and subsequent ultrasonic dispersion.

Apparent particle density and porosity values were taken from the report by (Pan et al., 2016), who used the same PAC that was used in the current experiments.

The diffusivity of MIB was estimated by means of the Hayduke–Laudie correlation method (Lyman et al., 1990). The same diffusivity value was used for EBC because the molecular sizes of EBC and MIB were assumed to be similar.

The rate constant for loss of MIB due to volatilization was determined by substituting the $C_{MIB}/C_{IN,MIB}$ value observed in the SMHS experiment without AC (Fig. 5S) into the following equation:

$$\frac{C_{MIB}}{C_{IN,MIB}} = \frac{1}{1 + K_{LA,i}\,V/Q} \tag{18S}$$

The effective HRT was determined by the result shown in Fig. 5S.

Table 6S. Tortuosity calculation

Parameter	Value	Origin
D_P	3.5×10^{-6} cm^2/s	from model fit (setting F)
Diffusivity in water, D_M		$D_M = 6.65 \times 10^{-6}$ cm^2/s
Tortuosity, τ	1.9	$\tau = D_M / D_P$

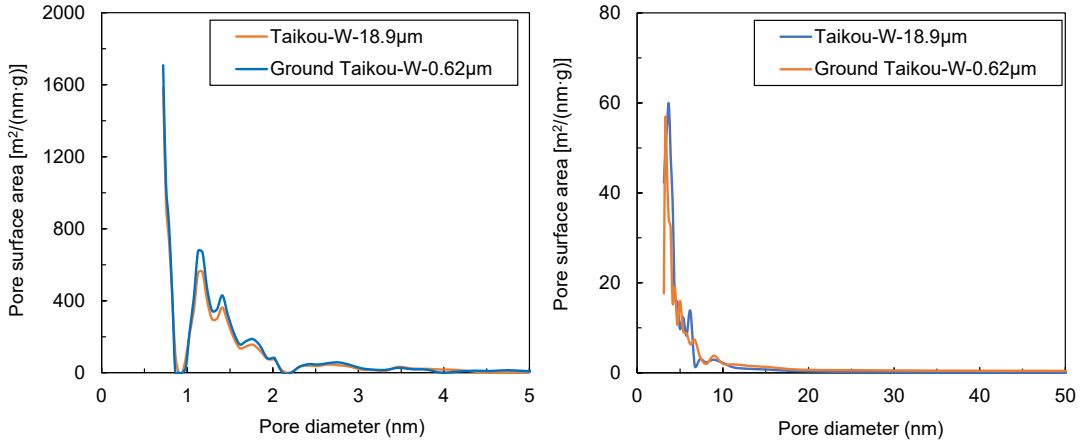

Fig. 1S. Pore size distributions of Taikou-W and Ground Taiko-W. The data is taken from the paper of Matsui et al. (2015).

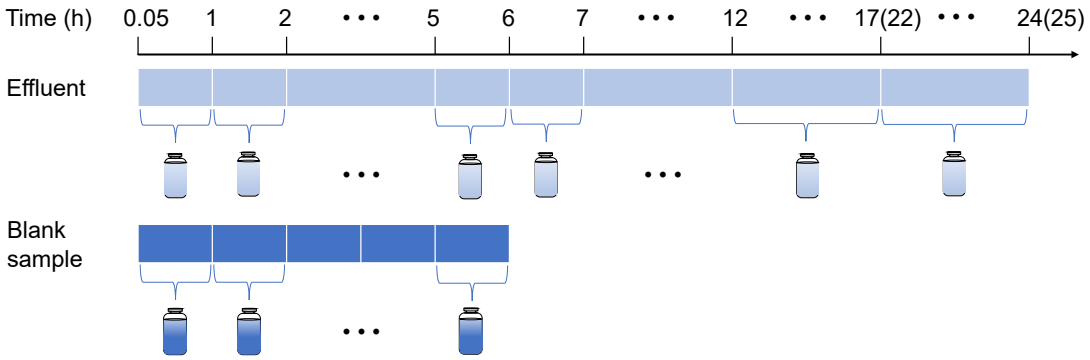

Fig. 2S. Sampling schedule.

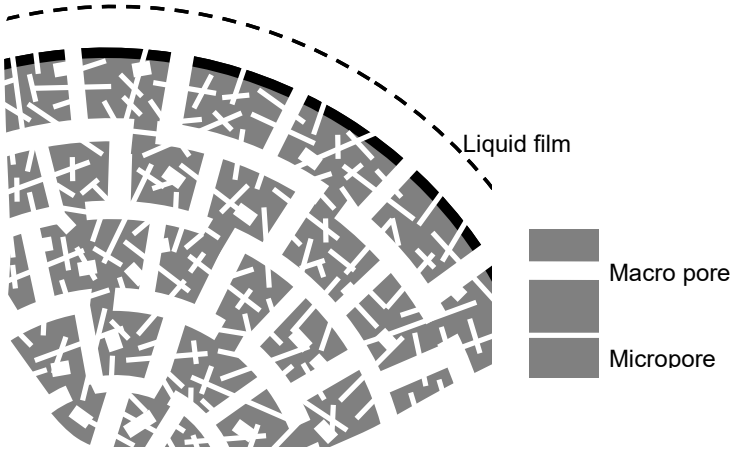

Fig. 3S. Idealized structure of activated carbon pore in BPKM (Matsui et al., 2009)

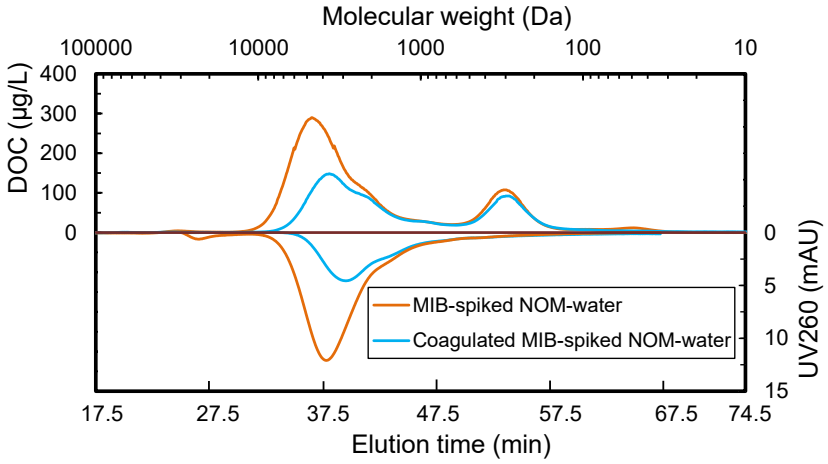

Fig. 4S. Molecular weight distributions of NOM in MIB-spiked NOM-water and Coagulated MIB-spiked NOM-water.

An HPLC system (1100 series, Agilent Tech, Tokyo, Japan) equipped with a single column (Toyopearl HW-50S, 250 mm × 20 mm, Tosoh Inc., Tokyo, Japan), an injection system (injection rate, 1.2 mL/min), a UV detector, and a total organic carbon analyzer (Sievers M9e, SUEZ, via Central Kagaku Corp., Tokyo, Japan) were used to determine the molecular weight distributions (Huber et al., 2011). The DOC analyzer equipped with degasser to eliminate inorganic carbon was connected to HPLC. The DOC analyzer continuously output the electric current value, which was corresponding to organic carbon concentration in the wet oxidation reaction vessel in the DOC analyzer.

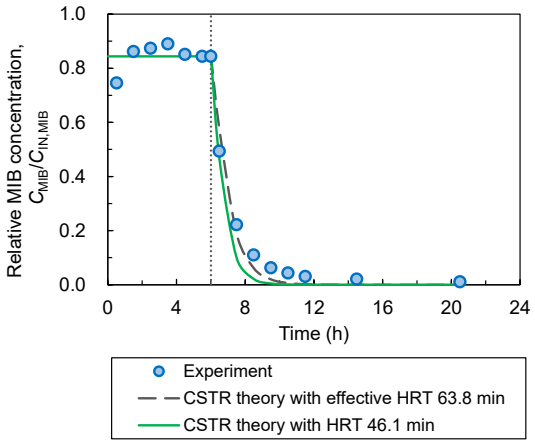

Fig. 5S. Time course of effluent/influent MIB concentration ratio ($C_{MIB}/C_{IN,MIB}$) in the SMHS with no AC. Influent containing ~1 μg/L MIB (Coagulated MIB-spiked NOM-water) was replaced by MIB-free water (Coagulated NOM-water) at 6 h (vertical dashed line). CSTR refers to continuous stirred-tank reactor.

In the absence of AC, the MIB concentration in the effluent of the SMHS was 15.6% lower than in the influent. Considering that the MIB concentration in the absence of AC was consistently 15.6% lower throughout the run rather than increased with time, we attributed the reduction to volatilization rather than to adsorption on the tank surface etc. In any case, the degree of adsorption, if any, would have been limited during the early stages of the experiment. This 15.6% value was used to determine the rate constant ($K_{LA,i}$) for loss of MIB due to volatilization in equation 18S.

After 6 h, there was a little difference between the measured MIB concentrations (solid line) and the concentration estimated by the CSTR theory (dot-dashed line) with the hydraulic retention time (HRT) of 46.1 min. However, the best fit was obtained with the effective HRT of 63.8 min, which was then used in the model simulations of MIB adsorption-desorption on PAC/SPAC in the SMHS.

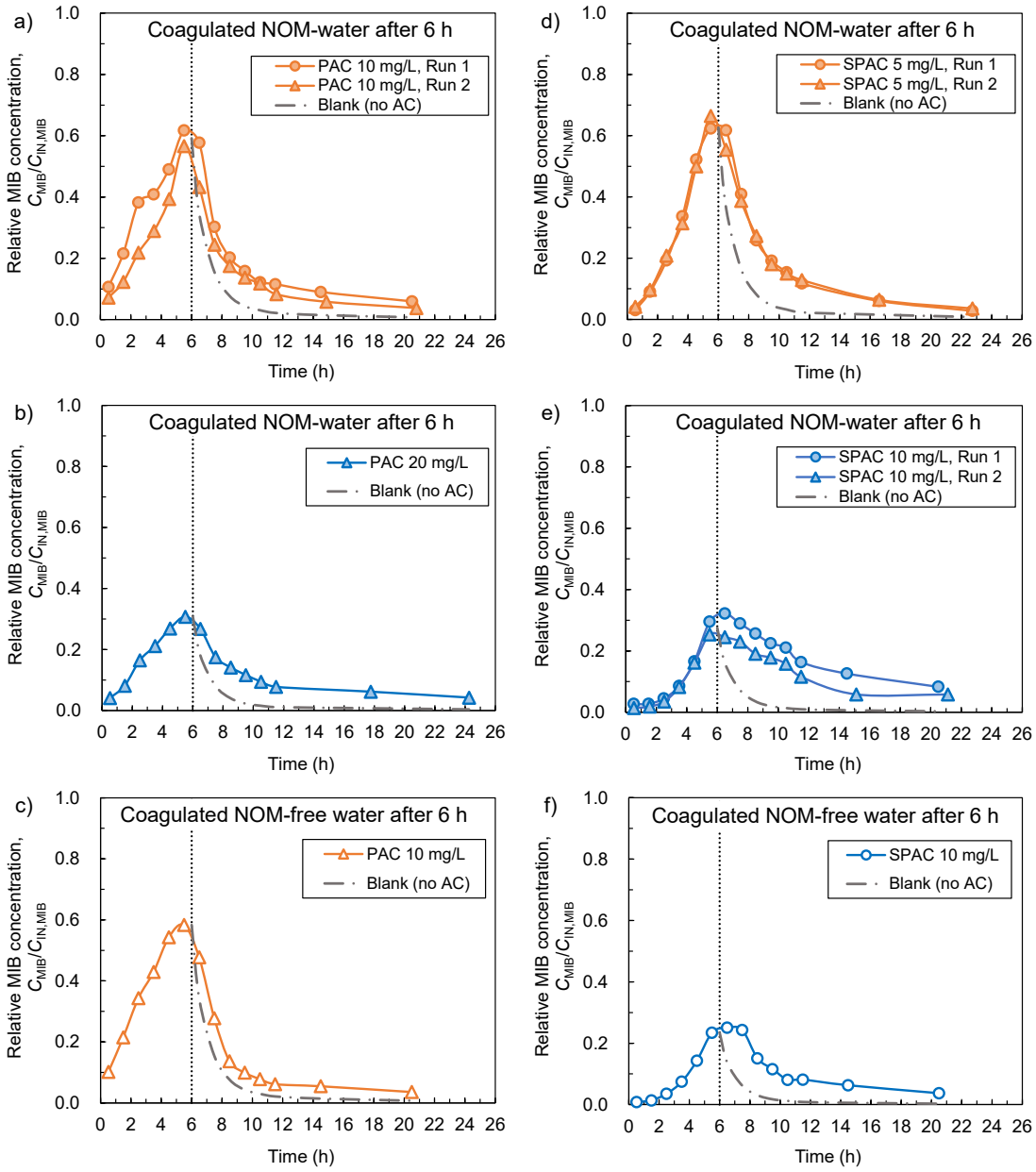

Fig. 6S. Time course of effluent/influent MIB concentration ratios ($C_{MIB}/C_{IN,MIB}$) in the SMHS with PAC (left) and SPAC (right). The plots connected by the solid lines indicate experimental data. The dot-dashed lines indicate estimates made by assuming that the AC was taken out from the SMHS at 6 h. The MIB-containing influent (Coagulated MIB-spiked NOM-water, $C_{IN,MIB} \approx 1$ μg/L) was replaced with MIB-free water (either Coagulated NOM-water or Coagulated NOM-free water) at 6 h (vertical dotted lines).

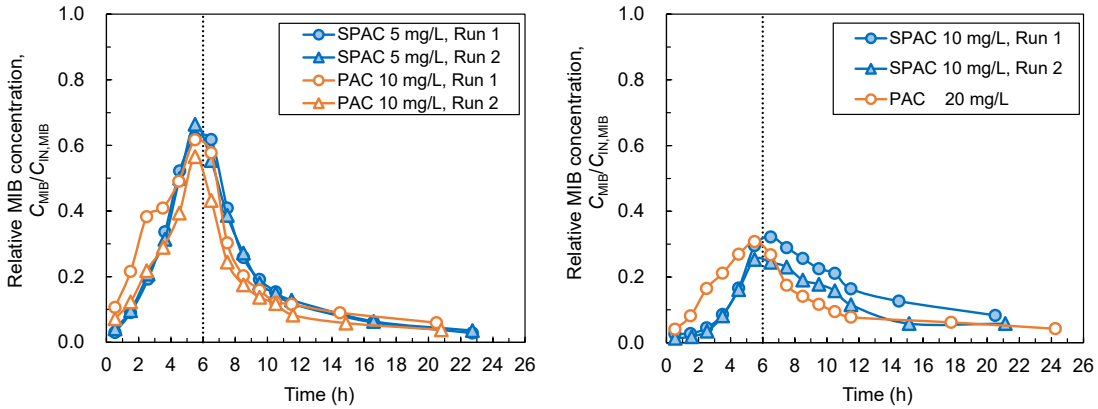

Fig. 7S. Time course of effluent/influent MIB concentration ratios in the SMHS-PAC/SPAC at lower (left) and higher (right) carbon dosages under the same influent conditions. The MIB-containing influent (Coagulated MIB-spiked NOM-water) was replaced with MIB-free influent (Coagulated NOM-water) at 6 h (vertical dotted lines). The x-axis values of the plots are times in the middle of each sampling period.

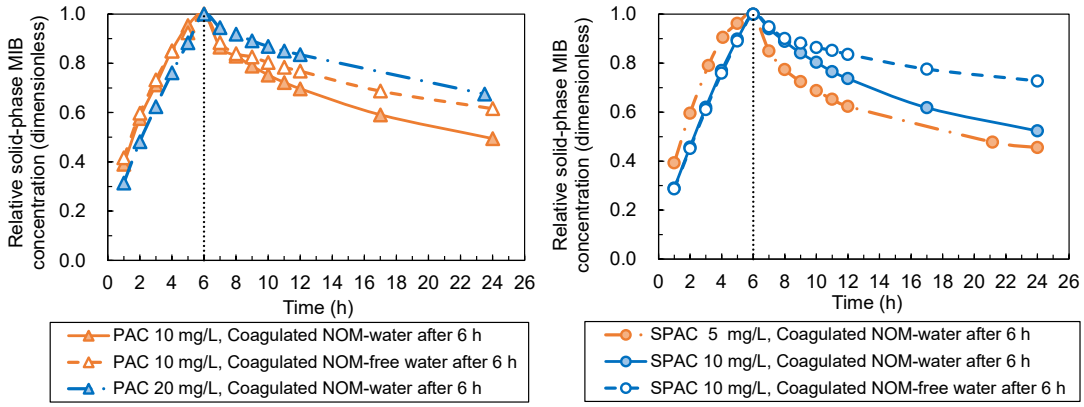

Fig. 8S. Time course of solid-phase MIB concentrations relative to each solid-phase MIB concentration before the start of the no-contamination period (6 h) for PAC (left) and SPAC (right). Influent containing ~1 μg/L MIB (Coagulated MIB-spiked NOM-water), was replaced by MIB-free influent (either Coagulated NOM-water or Coagulated NOM-free water) at 6 h (vertical dotted lines).

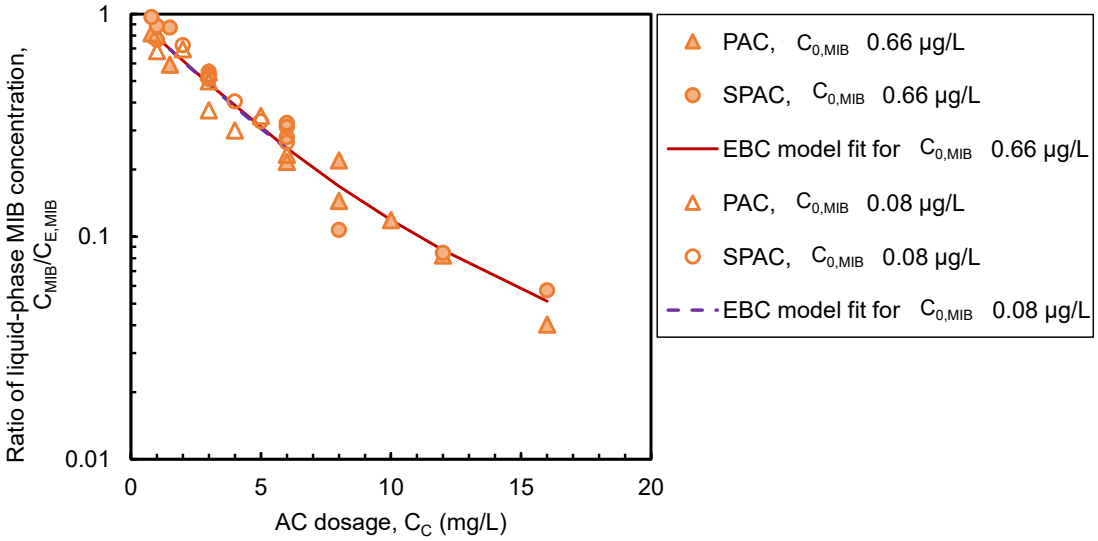

Fig. 9S. Ratio of equilibrium liquid-phase MIB concentration to initial MIB concentration ($C_{E,MIB}/C_{0,MIB}$) as a function of SPAC and PAC dosages for Coagulated MIB-spiked NOM-water. The initial MIB concentration are 0.08 or 0.66 µg/L. The lines are fits to the EBC (equivalent background compound) model under the fitting conditions listed in Table 2.

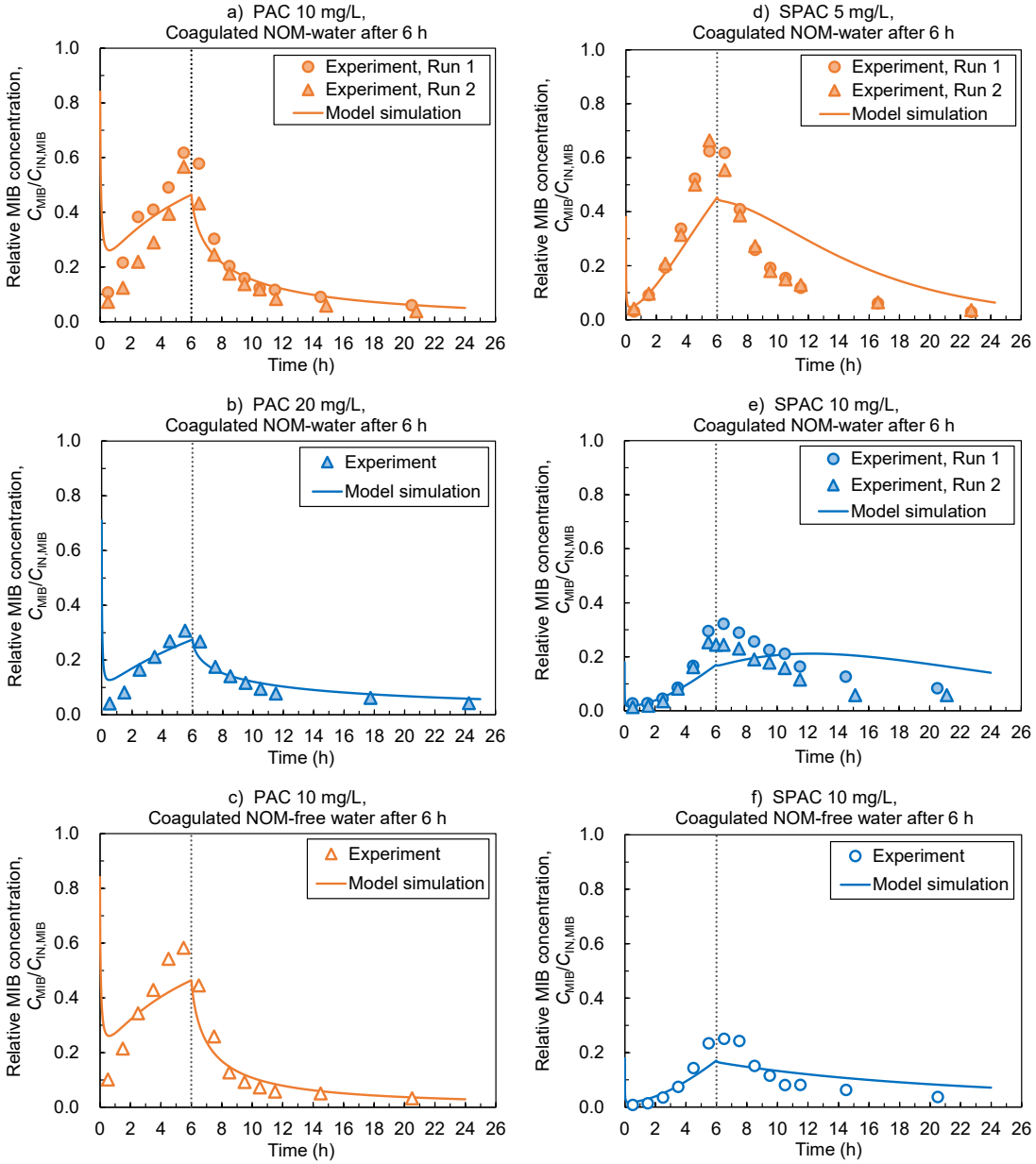

Fig. 10S. Comparison of experimental and simulated time courses of effluent/influent MIB concentration ratios ($C_{MIB}/C_{IN,MIB}$) in the SMHS with PAC (left panels) and SPAC (right panels). Simulations were conducted using setting A. The MIB-containing influent was replaced by MIB-free influent at 6 h (vertical dotted lines).

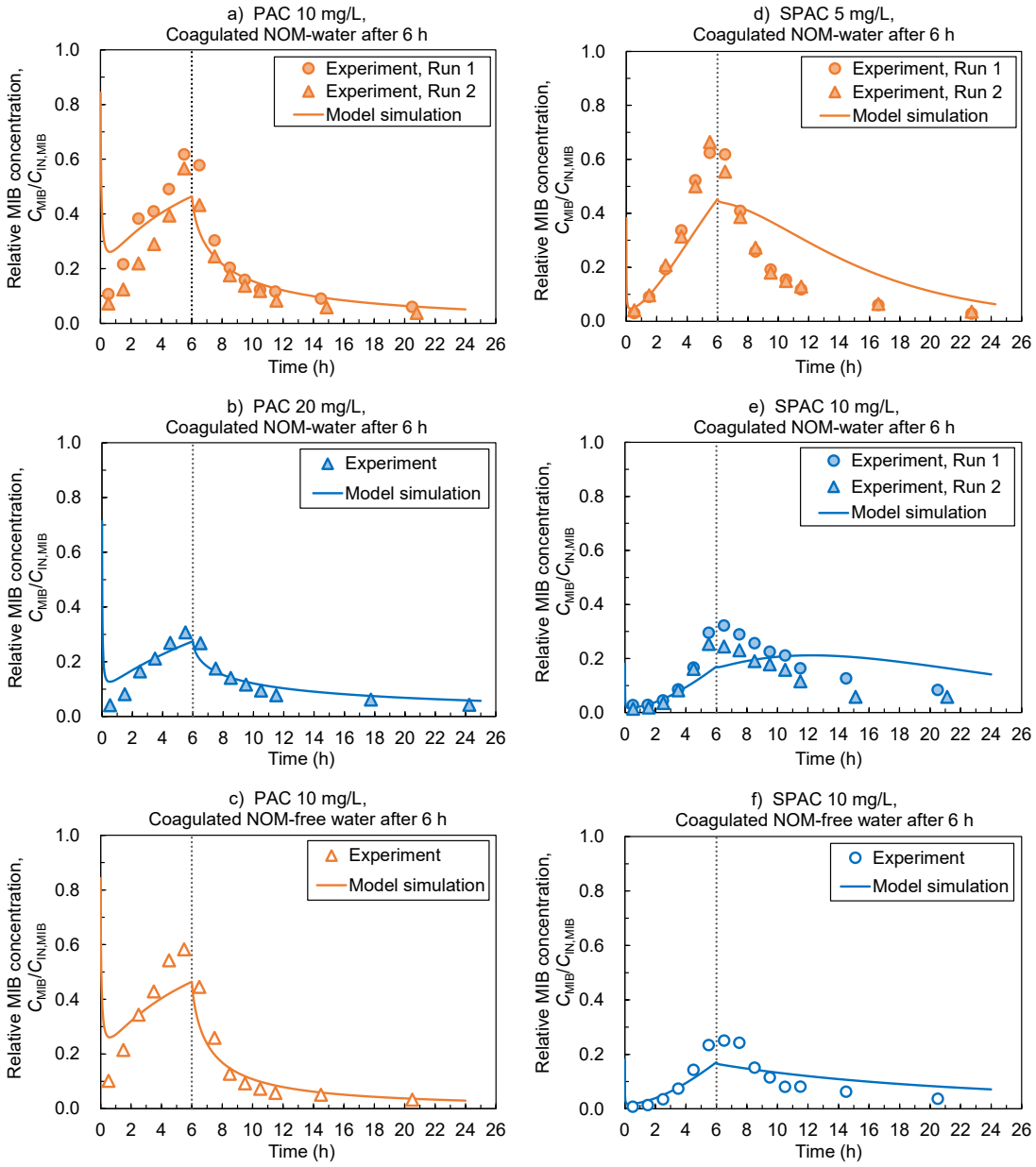

Fig. 11S. Comparison of experimental and simulated time courses of effluent/influent MIB concentration ratios ($C_{MIB}/C_{IN,MIB}$) in the SMHS with PAC (left panels) and SPAC (right panels). Simulations were conducted using setting B. The MIB-containing influent was replaced by MIB-free influent at 6 h (vertical dotted lines).

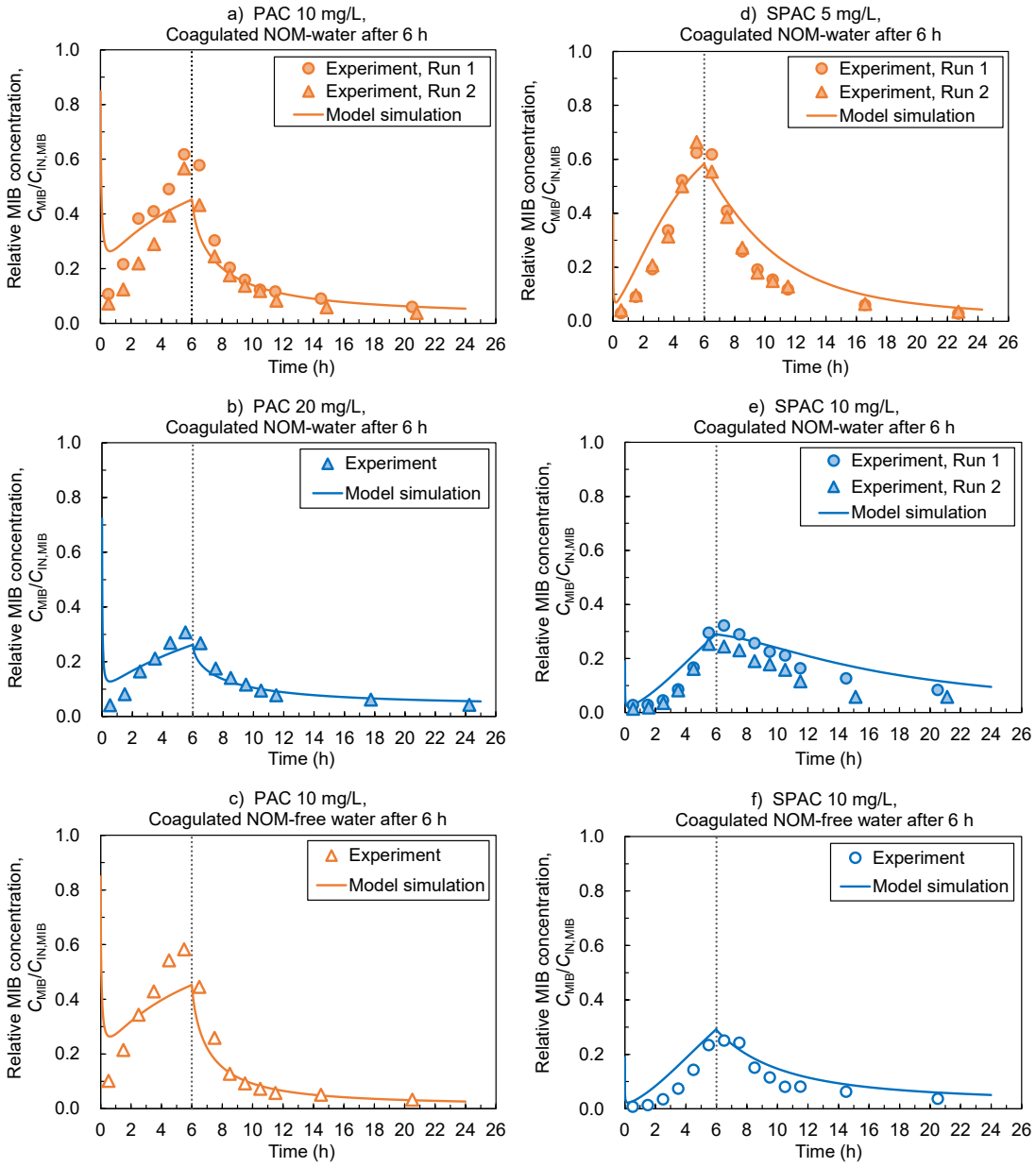

Fig. 12S. Comparison of experimental and simulated time courses of effluent/influent MIB concentration ratios ($C_{MIB}/C_{IN,MIB}$) in the SMHS with PAC (left panels) and SPAC (right panels). Simulations were conducted using setting C. The MIB-containing influent was replaced by MIB-free influent at 6 h (vertical dotted lines).

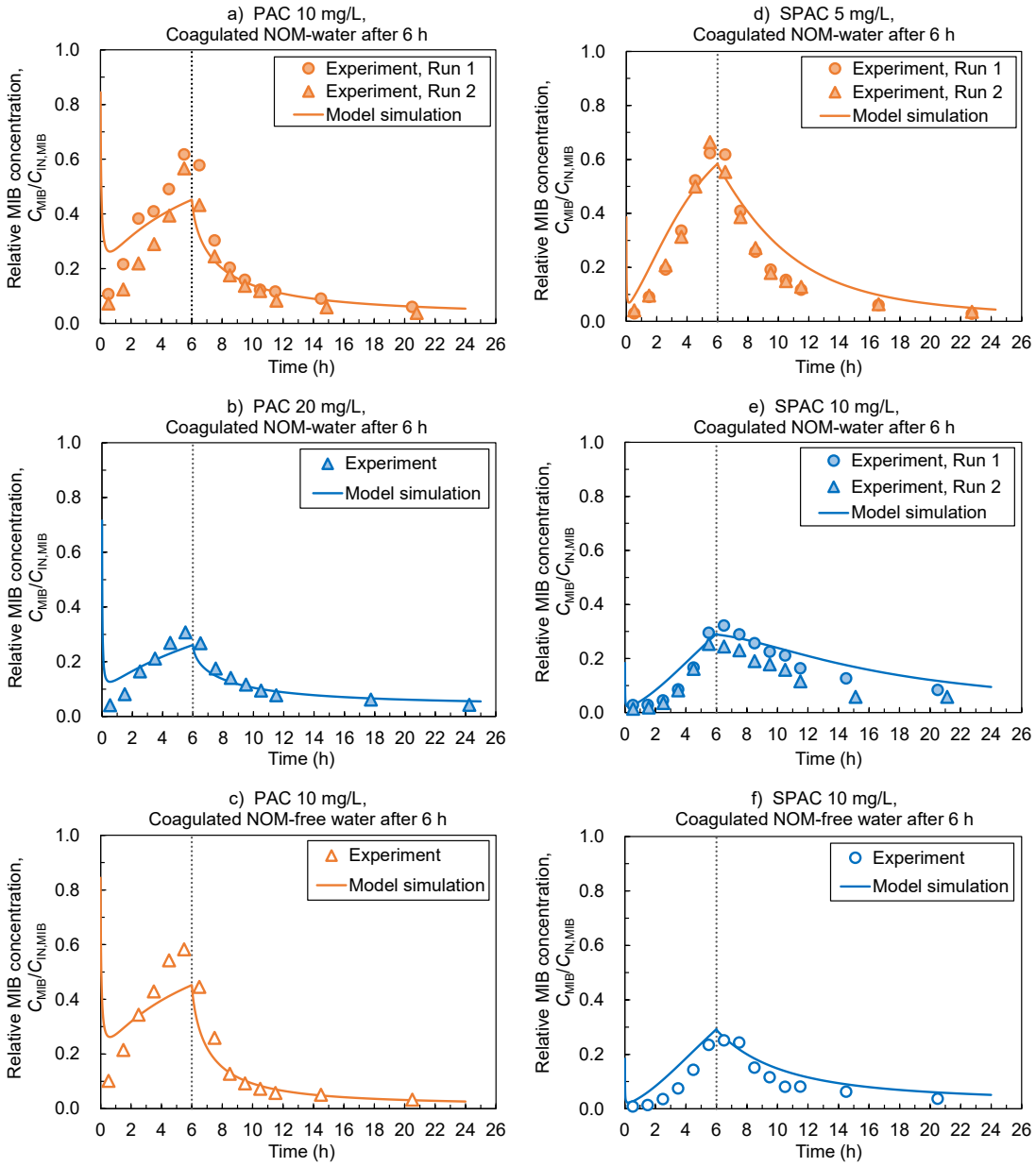

Fig. 13S. Comparison of experimental and simulated time courses of effluent/influent MIB concentration ratios ($C_{MIB}/C_{IN,MIB}$) in the SMHS with PAC (left panels) and SPAC (right panels). Simulations were conducted using setting D. The MIB-containing influent was replaced by MIB-free influent at 6 h (vertical dotted lines).

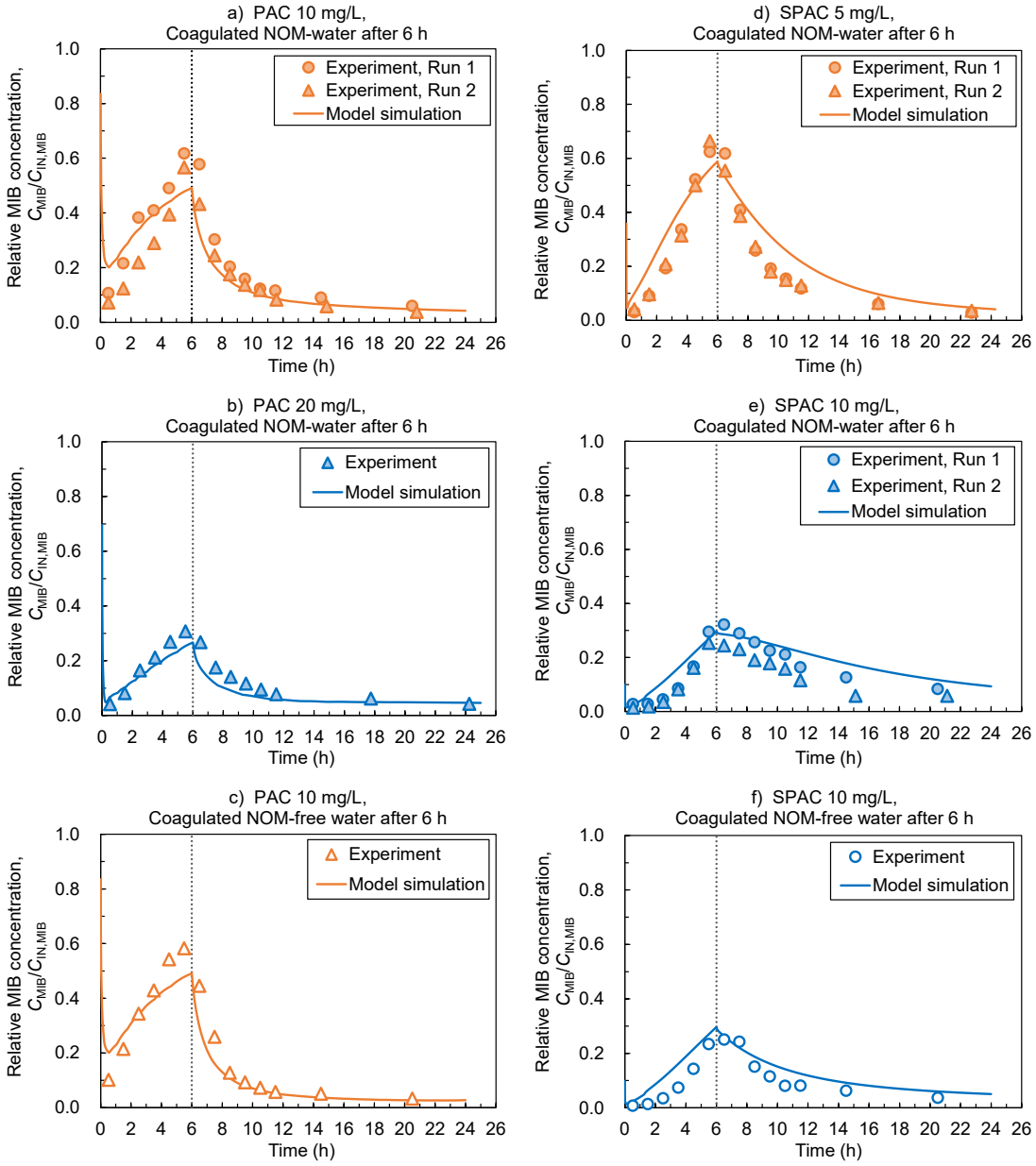

Fig. 14S. Comparison of experimental and simulated time courses of effluent/influent MIB concentration ratios ($C_{MIB}/C_{IN,MIB}$) in the SMHS with PAC (left panels) and SPAC (right panels). Simulations were conducted using setting E. The MIB-containing influent was replaced by MIB-free influent at 6 h (vertical dotted lines).

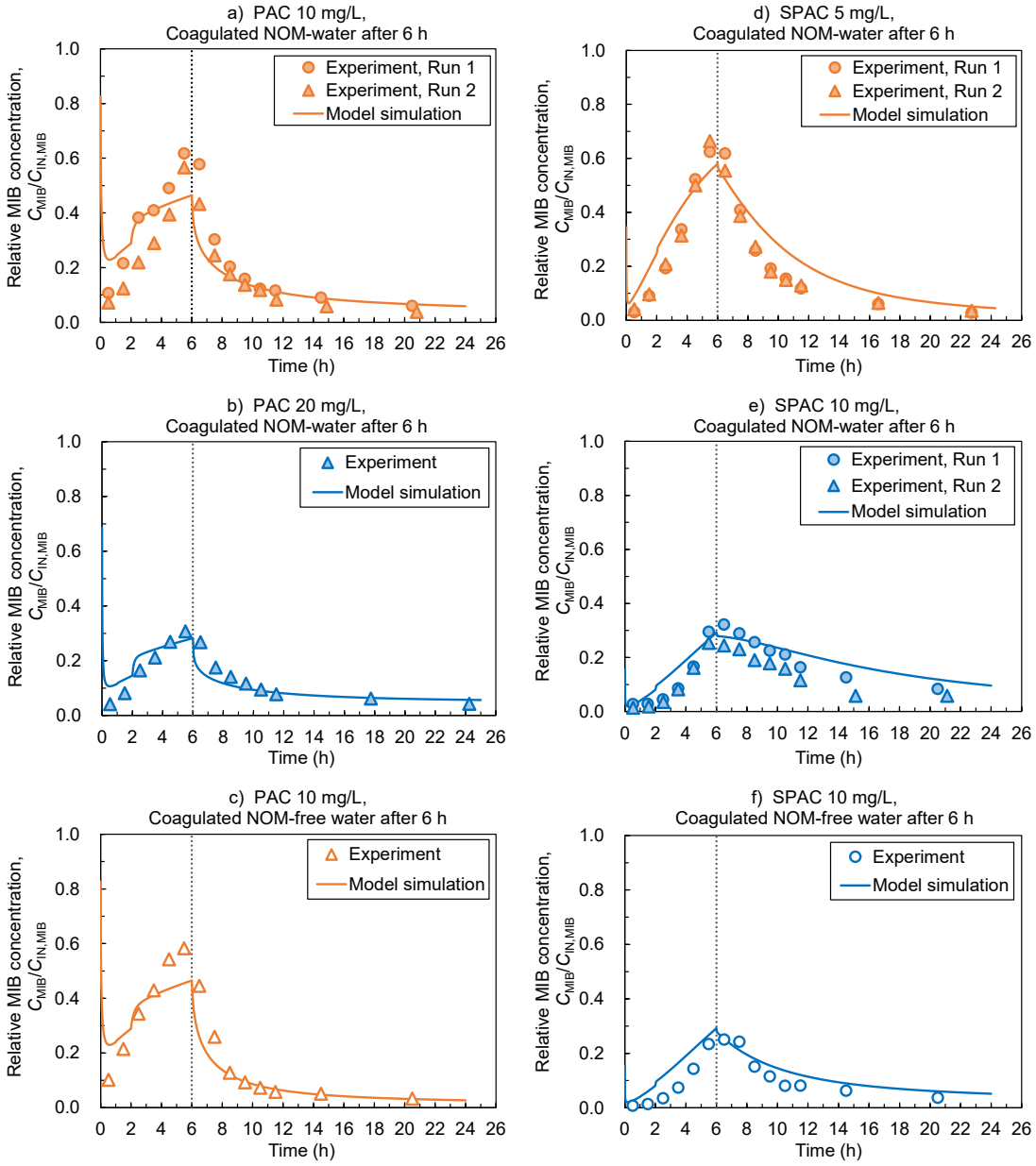

Fig. 15S. Comparison of experimental and simulated time courses of effluent/influent MIB concentration ratios ($C_{MIB}/C_{IN,MIB}$) in the SMHS with PAC (left panels) and SPAC (right panels). Simulations were conducted using setting G. The MIB-containing influent was replaced by MIB-free influent at 6 h (vertical dotted lines).

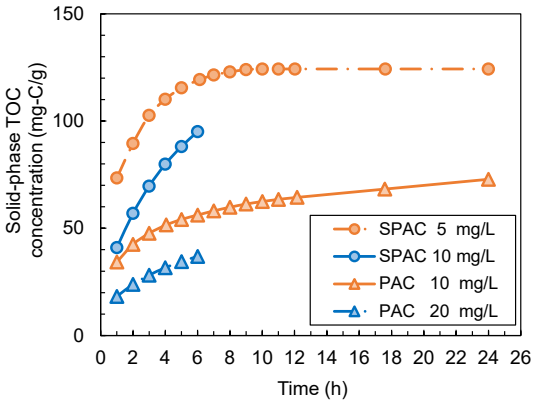

Fig. 16S. Time course of solid-phase TOC concentrations (i.e., TOC adsorbed on AC) in SMHS with PAC and SPAC.

References

Akaike, H. 1974. A new look at the statistical model identification. IEEE Transactions on Automatic Control 19(6), 716-723.

Burnham, K.P. and Anderson, D.R. (2002) Model selection and multi-model inference A Practical Information-Theoretic Approach, Springer.

Crittenden, J.C., Luft, P. and Hand, D.W. 1985. Prediction of multicomponent adsorption equilibria in background mixtures of unknown composition. Water Research 19(12), 1537-1548.

Edzwald, J.K. (2010) Water Quality and Treatment A Handbook on Drinking Water, McGrawHill.

Graham, M.R., Summers, R.S., Simpson, M.R. and MacLeod, B.W. 2000. Modeling equilibrium adsorption of 2-methylisoborneol and geosmin in natural waters. Water Research 34(8), 2291-2300.

Hand, D.W., Loper, S., Ari, M. and Crittenden, J.C. 1985. Prediction of multicomponent adsorption equilibria using ideal adsorbed solution theory. Environmental science & technology 19(11), 1037-1043.

Hepplewhite, C., Newcombe, G. and Knappe, D. 2004. NOM and MIB, who wins in the competition for activated carbon adsorption sites? Water Science and Technology 49(9), 257-265.

Ho, L. and Newcombe, G. 2005. Effect of NOM, turbidity and floc size on the PAC adsorption of MIB during alum coagulation. Water Research 39(15), 3668-3674.

Huber, S.A., Balz, A., Abert, M. and Pronk, W. 2011. Characterisation of aquatic humic and non-humic matter with size-exclusion chromatography – organic carbon detection – organic nitrogen detection (LC-OCD-OND). Water Research 45(2), 879-885.

IHSS Elemental Compositions and Stable Isotopic Ratios of IHSS Samples, International Humic Substances Society.

Kilduff, J.E. and Karanfil 1998. TCE adsorption by GAC preloaded with humic substances. Journal - American Water Works Association 90(5), 76.

Knappe, D.R.U., Matsui, Y., Snoeyink, V.L., Roche, P., Prados, M.J. and Bourbigot, M.-M. 1998. Predicting the Capacity of Powdered Activated Carbon for Trace Organic Compounds in Natural Waters. Environmental Science & Technology 32(11), 1694-1698.

Lyman, W.J., Reehl, W.F. and Rosenblatt, D.H. (1990) Handbook of chemical property estimation methods: environmental behavior of organic compounds, American Chemical Society, USA.

Matsui, Y., Ando, N., Sasaki, H., Matsushita, T. and Ohno, K. 2009. Branched pore kinetic model analysis of geosmin adsorption on super-powdered activated carbon. Water Research 43(12), 3095-3103.

Matsui, Y., Fukuda, Y., Inoue, T. and Matsushita, T. 2003. Effect of natural organic matter on powdered activated carbon adsorption of trace contaminants: characteristics and mechanism of competitive adsorption. Water Research 37(18), 4413-4424.

Matsui, Y., Nakao, S., Sakamoto, A., Taniguchi, T., Pan, L., Matsushita, T. and Shirasaki, N. 2015. Adsorption capacities of activated carbons for geosmin and 2-methylisoborneol vary with activated carbon particle size: Effects of adsorbent and adsorbate characteristics. Water Research 85, 95-102.

Matsui, Y., Yoshida, T., Nakao, S., Knappe, D.R.U. and Matsushita, T. 2012. Characteristics of competitive adsorption between 2-methylisoborneol and natural organic matter on superfine and conventionally sized powdered activated carbons. Water Research 46(15), 4741-4749.

Najm, I.N., Snoeyink, V.L. and Richard, Y. 1991. Effect of Initial Concentration of a SOC in Natural Water on Its Adsorption by Activated Carbon. Journal - American Water Works Association 83(8), 57-63.

Newcombe, G., Drikas, M. and Hayes, R. 1997. Influence of characterised natural organic material on activated carbon adsorption: II. Effect on pore volume distribution and adsorption of 2-methylisoborneol. Water Research 31(5), 1065-1073.

Newcombe, G., Morrison, J., Hepplewhite, C. and Knappe, D.R.U. 2002. Simultaneous adsorption of MIB and NOM onto activated carbon: II. Competitive effects. Carbon 40(12), 2147-2156.

Pan, L., Matsui, Y., Matsushita, T. and Shirasaki, N. 2016. Superiority of wet-milled over dry-milled superfine powdered activated carbon for adsorptive 2-methylisoborneol removal. Water Research 102, 516-523.

Peel, R.G., Benedek, A. and Crowe, C.M. 1981. A branched pore kinetic model for activated carbon adsorption. AIChE Journal 27(1), 26-32.

Qi, S., Schideman, L., Mariñas, B.J., Snoeyink, V.L. and Campos, C. 2007. Simplification of the IAST for activated carbon adsorption of trace organic compounds from natural water. Water Research 41(2), 440-448.

Schwarz, G. 1978. Estimating the Dimension of a Model. Ann. Statist. 6(2), 461-464.

Sidney Seckler, F.F., Margarida, M. and Rosemeire, A.L. 2013. Interference of iron as a coagulant on MIB removal by powdered activated carbon adsorption for low turbidity waters. Journal of Environmental Sciences 25(8), 1575-1582.

Sontheimer, H., Crittenden, J.C., Summers, R.S., Hubele, C., Roberts, C. and Snoeyink, V.L. (1988) Activated carbon for water treatment, DVGW-Forschungsstelle, Engler-Bunte-Institut, Universitaet Karlsruhe (TH), Karlsruhe.

To, P.C., Mariñas, B.J., Snoeyink, V.L. and Ng, W.J. 2008a. Effect of pore-blocking background compounds on the kinetics of trace organic contaminant desorption from activated carbon. Environmental science & technology 42(13), 4825-4830.

To, P.C., Mariñas, B.J., Snoeyink, V.L. and Ng, W.J. 2008b. Effect of strongly competing background compounds on the kinetics of trace organic contaminant desorption from activated carbon. Environmental science & technology 42(7), 2606-2611.

Villadsen, J.V. and Stewart, W.E. 1967. Solution of boundary-value problems by orthogonal collocation. Chemical Engineering Science 22(11), 1483-1501.